LBL-198
c.2

TRANSITION FROM BULK BEHAVIOR TO JOSEPHSON-JUNCTION LIKE BEHAVIOR IN SUPERCONDUCTING MICROBRIDGES

Yeong-du Song
(Ph. D. Thesis)

November 1971

AEC Contract No. W-7405-eng-48

TWO-WEEK LOAN COPY

This is a Library Circulating Copy which may be borrowed for two weeks. For a personal retention copy, call Tech. Info. Division, Ext. 5545

LAWRENCE BERKELEY LABORATORY
UNIVERSITY OF CALIFORNIA
BERKELEY

LBL-198
c.2

DISCLAIMER

This document was prepared as an account of work sponsored by the United States Government. While this document is believed to contain correct information, neither the United States Government nor any agency thereof, nor the Regents of the University of California, nor any of their employees, makes any warranty, express or implied, or assumes any legal responsibility for the accuracy, completeness, or usefulness of any information, apparatus, product, or process disclosed, or represents that its use would not infringe privately owned rights. Reference herein to any specific commercial product, process, or service by its trade name, trademark, manufacturer, or otherwise, does not necessarily constitute or imply its endorsement, recommendation, or favoring by the United States Government or any agency thereof, or the Regents of the University of California. The views and opinions of authors expressed herein do not necessarily state or reflect those of the United States Government or any agency thereof or the Regents of the University of California.

Table of Contents

Abstract v

I. Introduction 1

II. Experimental 5

A. Sample Preparation 5

B. Cryogenics and Magnetic Shielding 8

C. Microwave Cavity and Sample Holder System 10

III. Supercurrents at Zero Voltage 15

A. Solutions of the G - L Equations in the Microbridges . . 15

B. Critical Current Density in Superconductors 19

C. Experimental Results and Discussions 21

1. Temperature Dependence of the Critical Current . . . 21

a. Experimental results. 21

b. Discussions of the experimental results 23

c. Penetration depth correction 28

2. Magnetic Field Dependence of the Critical Currents . 29

a. Critical current of single bridge. 29

b. Critical current modulation of double bridge . . 31

IV. Current Voltage Characterisitcs at Finite Voltage 33

A. Undriven Mode 33

B. Driven Mode 39

V. Summary and Conclusions 42

Acknowledgements 45

References 46

Figure Captions 50

TRANSITION FROM BULK BEHAVIOR TO JOSEPHSON-JUNCTION LIKE BEHAVIOR IN SUPERCONDUCTING MICROBRIDGES

Yeong-du Song

Inorganic Materials Research Division, Lawrence Berkeley Laboratory
and Department of Nuclear Engineering, College of Engineering;
University of California, Berkeley, California

ABSTRACT

The behavior of superconducting microbridges has been studied as a function of the temperature, size and impurity dependent coherence length ξ of the evaporated film and the bridge length L. When $L \ll \xi$ near the transition temperature T_c, the ac and dc supercurrents in the bridge have a Josephson-junction like behavior. When $L \gg \xi$, the bridge behaves like a bulk superconductor. Continuous transitions from the bulk behavior to a Josephson junction like behavior are observed as a function of L/ξ by varying the temperature or the mean free path. Experimental results of the temperature dependence of the critical current are very well explained by the one-dimensional model of Baratoff et al.

The finite voltage I-V characteristics are qualitatively analyzed by the lumped circuit parameter model. The microwave power dependence of the height of the induced current steps is in good agreement with the calculation in the limit where the bridge shows Josephson junction like behavior.

I. INTRODUCTION

A superconductor is in a macroscopic quantum state[1] which can be described by a single wave function assigned to a macroscopic number of superconducting electrons. This wave function is represented by a complex order parameter $\psi = \sqrt{\rho_s}\ \exp(i\phi)$ given by the phenomenological theory of Ginzburg and Landau,[2] where ρ_s is the density of the superconducting electrons and ϕ is the phase of the order parameter. The phenomenological theory has been derived, from the microscopic theory, and the derivation has shown that the order parameter $\psi(\underset{\sim}{r})$ is proportional to the energy gap parameter $\Delta(\underset{\sim}{r})$.[3] Such an order parameter has a long range phase coherence within a superconductor, that is, to fix the value of the phase at one point determines its value at all other points, due to a cooperative effect brought about by the motion of the electrons from one part of a superconductor to another.

When two pieces of superconductor are isolated there is no current flowing between them, and hence no correlation between the phases of the order parameter in the two pieces. If these two pieces are joined by a superconducting wire, the system becomes effectively one superconductor and phase coherence extends from one piece to the other. The wire can carry a certain critical current before the phase coherence breaks down and a finite voltage develops across it.

Josephson initially predicted[4] the following effects for tunnel junctions and later extended[5,6] for general weak link systems with a much smaller critical current than the bulk value. First, a dc supercurrent flowing at zero voltage, given by

$$I = I_c \sin \phi \tag{1}$$

where (I_c) is the critical current density of the weak link and ϕ is the gauge invariant phase difference between the order parameter of two pieces of superconductor. At finite bias voltage V across the weak link, there is an ac supercurrent of frequency 2eV/h (483.6 MHz/μV) flowing in addition to the normal current. This prediction was followed by experimental confirmation of such effects on superconductor insulator superconductor (S-I-S) junctions,[7] superconductor normal superconductor (S-N-S) junctions,[8] point contacts[9] and superconducting microbridges.[10]

In a superconducting microbridge system, the role of the weak link is played by a short (~1μ), narrow (~1/2μ) bridge section existing between large patches of the film on either side. Since the bridge section has a non-negligible cross-sectional area of $\sim 10^{-13} m^2$, and consists of a superconducting material, the critical current carried by the bridge at low temperature (typically order of 10mA in our bridges) can be much larger than that set forth by Josephson as the criterion for satisfying the condition for weak links. The criterion is that the coupling energy, which is proportional to the critical current, be less than the Fermi energy. On the other hand, at high temperature, the critical current due to intrinsic bulk superconducting properties of the bridge is expected to be small and we may anticipate some enhancement of the critical

current due to the presence of strong superconductors with much higher critical current on either side of the bridge. Here "Strong" and "Weak" are used in connection with the critical-current-carrying capacity. Therefore, a superconducting microbridge is expected to behave like a bulk superconductor in the low temperature limit and like a Josephson junction at high temperatures at the right conditions. Incidentally, all of the reported observations of ac Josephson effect on the microbridge[10,11,12] were made in the high temperature limit. Since the original demonstration by Anderson and Dayem[10] that the microbridge exhibits ac interference effects, a considerable amount of effort has been concentrated on applications of the bridge, especially as a detector of high frequency electromagnetic fields. This trend of interests and some difficulties associated with the preparation of standard samples of ~1μ size has precluded any systematic study of the physical parameters which characterize the behavior of the bridge. The aim of our study is to undertake this investigation by varying the physical parameters of the bridge.

In section II, we will discuss the experimental techniques used in our experiments.

In section III, the temperature dependences of the critical currents of microbridges will be discussed in relation to the coherence length $\xi(T)$ of the strong superconductor on either side of the bridge. Coherence length was varied with temperature, with the thickness of the film, and with the impurity of the film. Also, the critical current of a single bridge and of a double bridge as a function of a perpendicular magnetic field will be discussed.

In section IV, the current-voltage characteristics in the absence, and in the presence of an 8.8GHz microwave field will be discussed using the lumped circuit parameter model.

In all cases, the detailed discussions will be done in two limiting cases; that is, when the microbridge behaves like a bulk superconductor and when it behaves like a Josephson junction. Continuous transitions of characteristics from one limit to the other were always realized in the actual experiments as we changed the physical parameters of the bridge continuously.

Section V includes the summary and conclusions drawn from our experiments.

II. EXPERIMENTAL

A. Sample Preparation

The Sn and Sn-In alloy bridges used in our experiments were prepared by vacuum deposition of thin films onto ordinary microscope cover glasses and, then, by scratching these films mechanically with a specially designed micromanipulator outside the vacuum. The Sn was chosen as a primary material because of the wide range of T/T_c readily attainable in a standard liquid-helium cryostat and the durable chemical and mechanical properties of the Sn film. Usually three longitudinal strips of 400μ width were deposited on one glass substrate. Film thickness varied from 500Å to 3000Å, evaporation pressure from 1 to 8×10^{-7} Torr, deposition rate from 5 to 50 Å/sec and substrate temperature from LN_2 temperature up to room temperature. Substrates were cleaned ultrasonically in soap and water for 15-20 minutes, then rinsed with the distilled water, acetone and ethyl alcohol in that order and finally were stored in ethyl alcohol. Occasional ultrasonic cleaning in the ethyl alcohol was sufficient to keep the substrates clean for months.

Discontinuity and surface roughness resulting from Sn agglomerating around clustering centers randomly distributed on the glass substrate was the main problem encountered in preparing uniform films.

Cooling the substrate at liquid nitrogen temperature during the evaporation and subsequent rapid warming up to room temperature prevented this non-uniformity. A cold substrate makes it difficult for

atoms to migrate to their favorite clustering centers. Rapid warming up of the substrate was necessary, because the gradually warmed up films acquired a white, milky and non-metallic appearance. For films thinner than about 800Å, it was impossible to obtain electrical continuity with evaporation to a room temperature substrate. The only other way to circumvent this problem was to use uncleaned substrates (fresh from the supplier's box), thus introducing uniformly distributed cluster centers, and to evaporate at high pressure ($\sim 1 \times 10^{-5}$ Torr) and at high deposition rates (~50Å/sec). We used the cooling method exclusively in preparing samples thinner than about 1000Å. The substrates were bonded with Apiezon N vacuum grease to a copper block which was chilled by the liquid nitrogen.

After the evaporation, the films were placed on the micromanipulator. The first scratch was made about half way across the width of the film by a commercially available fine point diamond tool. Then the tool was lifted up and the sample was translated the desired distance by the micromanipulator. Finally, the tool was lowered to finish the second scratch. The micromanipulator consisted of an aluminum block supported by four 1/2 in. aluminum rods and a 5 pounds per inch strenght coil spring. This pushes against the aluminum block, thereby causing elastic deformation of the supporting rods on a micron scale.

Bridge dimensions were normally measured under an optical microscope at X 1000 magnification with a calibrated filar micrometer having a resolution of ~0.2μ. They were typically of 1/2μ wide and 1μ

long. Fifteen out of more than 100 samples tested were observed under a scanning electron microscope (JSM-3) at a magnification between 3,000 and 10,000. This confirmed that the measurements done by the optical microscope were within ± 30% of the actual dimensions, and revealed the rough surface structure of the film deposited onto the substrate at the room temperature, as well as the piling up of the Sn along the scratched path. This resulted in about twice the deposited thickness at the bridge. Therefore, whenever estimating the cross-sectional area of the bridge, twice the film thickness was used for the bridge thickness. Taking the room temperature resistivity of Sn (11.5×10^{-8} Ω - m), residual resistivity ratio (R R R) of 20, (which was typical value observed for 2000Å thick Sn film) bridge cross-sectional area of $10 \times 10^{-14} m^2$ and length of 10^{-6} m, the calculated resistance was the right order of magnitude when compared to the value deduced from actual I-V curves. Resistance of the bridges at 1°K varied from .03 ohm to .5 ohm depending on the impurity and bridge dimensions.

After the bridge was formed in this way, the sample was installed on the sample holder inside the microwave cavity and the electrical leads were attached to the film using silver conducting paint.

The thickness of the film was continuously monitored during the evaporation by Sloan DTM-3 quartz crystal microbalance and the absolute thickness was determined with a Varian 980-4000 Fizeau interferometer using the monochromatic light of half wave length 2945Å from sodium vapor.

Sn and In make solid solutions at almost all concentrations[13] and up to about 3 at.% of In, the thermodynamic properties of the alloy are nearly same as pure Sn.[14,15] For instance, the superconducting transition temperature is slightly lowered to 3.63°K at 3 at.% In from 3.72°K for pure Sn, but In provides satisfactory scattering centers as may be seen from the RRR measurements. Above 3 at.%, Sn-In alloy goes into another phase which has superconducting transition temperature higher than 4.2°K. Since the melting points of the two materials differ by 80°C (for In 156.4°C and for Sn 231.9°C) and vapor pressures differ by 2 to 3 orders of magnitude, it is very difficult to predict the In concentration of a film evaporated from Sn-In alloy. We simply used trial and error until the desired concentration was achieved. To avoid processes like distillation by fractuation, rapid evaporation was necessary. Alloy films produced by this method ranged from RRR=20 to RRR=5 corresponding to the mean free path varying from 2000Å down to 400Å. Sn and In used in the experiments were 99.999% pure.

B. Cryogenics and Magnetic Shielding

A sketch of the dewar system is shown in Fig. 1.

Experiments were conducted using a standard glass liquid helium dewar of 10 cm inner diameter and 120 cm. height. The temperature was varied between 0.9°K and 4.2°K with a booster diffusion pump and a large mechanical pump. Temperature was regulated to within a few millidegree with an ac wheatstone bridge type temperature regulator using low noise operational amplifier circuits.[16] The sensing element was a 27 ohm, 1/8 Watt Allen-Bradley BB series carbon resistor and the heater current was fed back to 160 Ω manganin wire wrapped around the copper

can housing the microwave cavity.

The ambient magnetic field was shielded with high permeability shield material from Perfection Mica Company. The shield was 100 cm high and 32 cm in diameter, and was wrapped three times around the liquid nitrogen dewar. The magnetic field at the sample position was reduced to less than a few milligauss by this method.

Temperatures were measured with a germanium thermometer located at the center of the cavity tuning plunger. This was the closest available proximity to the sample without disturbing the microwave field inside the cavity. Considering that the critical current and microwave induced current steps are very sensitive functions of temperature in the superconducting microbridge near T_c and considering that the microwave power dissipated inside the cavity can be as much as a few milliwatts, large amounts of error could be introduced into the experimental results unless the thermometer was placed in very close proximity to the sample. Two thermometers, Solitron 1761 and Cryocal 988, were calibrated against the known primary standard of our laboratory[17] at more than fifty points between 0.9°K and 4.2°K. Their resistance values were fitted to the seven term logarithmic polynomials[18]

$$T^{-1} = \sum_{i=-1}^{5} a_i \, (\log_{10} R)^i \qquad (2)$$

where T is the temperature in °K and R is the resistance in ohms. Voltages were measured to five digits using a Leeds and Northrup K-5 potentiometer.

Root mean square deviation of the observed data from the fitted curve was less than ~2 mdeg K and less than ~3 mdeg K, respectively. Absolute temperatures were calibrated against the helium vapor pressure measured with a mercury manometer, and the discrepancies were typically less than 10 millidegrees. Resistances at helium temperature were 430.7 ohms and 572.1 ohms respectively and they increased by about an order of magnitude in going down to 1°K. It is estimated that these thermometers were accurate to an absolute value within ± 10 mdeg K.

C. Microwave Cavity and Sample Holder System

The microwave cavity and sample holder system used in our experiments were designed to provide the freedom of rotating and translating the samples inside the cavity, so that the bridge could be coupled to the microwave field selectively. Another advantage associated with the movable sample was that the sample itself acted as a tuner, thereby making it possible to enhance the power coupling into the cavity after the sample was installed and immersed in the liquid helium. As shown in Fig. 1, X-band wave guide coming down from the dewar flange was coupled into a cylindrical TE_{011} resonant cavity through a coupling hole of .28 in diameter located on the end walls of the wave guide and the cavity. The coupling was through H_{rf} linked between the wave guide and the cavity; therefore the hole was located at the position where H_{rf} was maximum in the wave guide and in the cavity, respectively.

The cylindrical TE_{011} mode has a field distribution such that E_{rf} is azimuthal and parallel to the end walls and H_{rf} is radial near the end walls and axial along the side walls and along the central axis. Since there is no rf current flowing across the end wall, the lower

end wall was made of a movable plunger to tune the cavity into resonance in the frequency range of 8GHz to 10GHz. Another of the advantages gained with this movable plunger is that all the other modes of resonance which do not have cylindrical symmetry or which require good electric contact between the end wall and the side wall are effectively suppressed.

The cavity diameter was 42 mm and the height of the plunger was 34 mm when it was resonating at 8.8 GHz, where the maximum power coupling was achieved. Usually the resonance frequency shifted to a slightly lower value upon the introduction of liquid helium into the cavity, due to a slight difference between the dielectric constants of liquid helium and that of vacuum.

The sample holder was introduced through a 3.2 mm diameter hole on the top end wall located at 0.48 X (radius) of the cavity from the center, where E_{rf} was maximum. The sample holder was made of a high W, low loss plastic material (Eccostock) from the Emerson and Cummings Co., and was designed to hold a 11 mm × 20 mm microscope cover glass, and was extended to the outside of the cavity where it joined a 3.2 mm diameter stainless steel sample control rod. Both the sample holder and the tuning plunger were controlled from outside the dewar.

The Q of the cavity and power reflection coefficient were measured simultaneously on an oscilloscope display of the detector (1N23B) output with the voltage sweeping the klystron (Varian X-12) frequency. Detector output was calibrated against a General Microwave 460 thermoelectric power meter and the sweep voltage was marked with pips generated by a reaction type frequency meter. The loaded Q of the

cavity, Q_L, is given by the relation

$$Q_L = \frac{f_o}{\Delta f} \tag{3}$$

where f_o is the resonant frequency of the cavity and Δf is the frequency band width such that at the frequency $f^{\pm} = f_o \pm \frac{\Delta f}{2}$, the power coupled into the resonator drops to 1/2 of its value at resonance. The coupling coefficient β is given by the voltage standing wave ratio at resonance with the relation

β = (VSWR) resonance if overcoupled

β = 1/(VSWR) resonance if undercoupled.

VSWR is related to the power reflection coefficient $|\rho|^2$ by

$$\text{VSWR} = \frac{(1 + |\rho|)^2}{(1 - |\rho|^2)} \tag{4}$$

The Q_o of this cavity (which was overcoupled) was calculated to be 1730 from the measured value of $Q_L \simeq 300$ and the power reflection coefficient of $\simeq 0.5$. Compared to the theoretically predicted value of $Q_o \simeq 10^4$ for a brass cavity having this geometry,[19] there was a considerable degradation of Q value; however, it was hardly unacceptable considering that a large portion of the cavity volume with strong E_{rf} was occupied by the sample, the wires attached to it, and sample holder. From the known field distribution and Q_o, the absolute value of the field strength can be calculated using the relation.

$$Q_o = \omega \frac{\text{Energy stored in the cavity}}{\text{Power dissipated in the cavity}} = \frac{\omega_o \int \mu H^2 d\tau}{P_d} \tag{5}$$

P_d, the power dissipated in the cavity is the difference between the power delivered to the cavity and the power reflected from it neglecting the attenuation along the waveguides.

The energy stored is simply the volume integral of the electromagnetic energy density in the cavity. Maximum magnetic and electric fields were calculated for $Q_o = 1730$, and they were

$$|H_{rf}|_{max}\ (\text{Oe}) = 1.01 \times 10^{-3} \sqrt{P_d\ (\mu w)}$$

$$|E_{rf}|_{max}\ (\mu V/\mu m) = 3.4 \times 10 \sqrt{P_d\ (\mu w)} \qquad (6)$$

The major source of error which could come in this estimate was the determination of the power reflection coefficient. Any kind of discontinuities along the wave guide can set up the reflection of the wave which enters the detector. Care was taken to cancel out these unwanted reflections whenever the Q measurements were made by setting up a counter reflection with the tuner.

A simplified schematic diagram of the microwave and measuring electronic circuit system is shown in Fig. 2. Microwaves generated by the Varian X-12 klystron were passed through the buffer attenuator and Hewlett Packard X382A precision attenuator and transmitted to the cavity. Power transmitted and power reflected were measured with 1N23B crystals mounted at the end of 20dB dual directional couplers. Relative input power was always measured by reading the setting of a precision attenuator.

The I-V characteristics of the microbridge were measured with a constant current biasing circuit. The output of the Wavetek function generator was passed through a low pass filter, followed by a current limiting resistor, R_I, which varied from 100 Ω to 1 Meg Ω depending on the magnitude of the current needed. The constant current bias condition was still satisfied even at R_I = 100 Ω since the bridge resistance was typically 50m Ω. The voltage drop across a 0.1% precision current measuring resistor in series with the bridge was fed into the Y input of the display system. Bridge voltage was first amplified with a Hewlett Packard 7785 differential amplifier and was fed into the X input of the display system.

Two different sets of coils were used to provide the static magnetic field up to ~10G at the sample. One set was simply wrapped around the cylindrical cavity and used with the microwave experiment, while the other set was two pairs of Helmholtz coils which were used in the critical current modulation experiment. In the first case, the field strength was taken from a table.[20] Both sets of coils were housed inside the liquid helium dewar.

III. SUPERCURRENTS AT ZERO VOLTAGE

One of the basic properties common to various systems of weakly coupled superconductors is that there exists a well defined critical current on the order of milliamperes, above which the phase coherence between the two superconductors breaks down and a finite voltage develops between them.[5] This critical current is a measure of the coupling energy between the two superconductors, and provides ~2 eV of coupling energy per 1 mA of critical current. In the superconductor insulator superconductor (S-I-S) junctions, the supercurrent flows by tunneling as described by the tunneling Hamiltonian.[4,21] In the superconductor normal superconductor (S-N-S) junctions supercurrent flows by the proximity effects[22] due to the overlap of the superconducting wave functions inside the normal metal which tail exponentially from from the adjacent superconductors. The supercurrent flow mechanism in the superconducting microbridge is simpler, i.e. supercurrent flows inside the superconductor. The relevant equations describing these phenomena are given by Ginzburg and Landau,[2] and it is necessary to look for the solutions of the Ginzburg-Landau (G - L) equations in the microbridges to show why they exhibit weak link behavior.

A. Solutions of the G - L Equations in the microbridges

Analytic solutions of the G-L equations for the one-dimensional model of short superconducting weak links have been obtained by Baratoff, Blackburn, and Schwartz.[23] Similar solutions have also been obtained for a slightly different model by Christiansen, Hansen, and

Sjöström.[24] The main difference is that the former solved the equations for the entire region of the weakly coupled superconductors, namely, the weak link with a bulk superconductor on either side, while the latter considered the solution in the weak link region only. We will follow the model of Baratoff et al. which visualizes the continuous change of the order parameter across the links more clearly than that of Christianser et al.

Figure 3a is a sketch of a physical real microbridge of width W and length L, while Fig. 3b is the corresponding one-dimensional model. The bridge has a lower critical-current-carrying capacity than the superconductors on either side, but is assumed to have the same thermodynamic properties such as transition temperature T_c, equilibrium energy gap Δ_o, and bulk critical field H_c. On conformally transforming to the geometry of the one-dimensional model, the bridge region (S_B) is enlarged to the same cross-sectional area as the superconductors on either side (S_A) and hence a smaller critical current density, which in turn imples a shorter mean free path in the S_B region. Let the origin of the one-dimensional co-ordinate x be at the middle of S_B. The region S_B ($|x| < L/2$) has a shorter mean free path ℓ_B than in the region S_A ($|x| > L/2$) and hence a longer penetration depth $\lambda_B = \lambda_A/\gamma^{1/2}$ and a shorter coherence length $\xi_B = \xi_A\,\gamma^{1/2}$. Here $\gamma = \chi_B/\chi_A$ and χ is Gor'kov's[25] universal function of the impurity parameter, ξ_o/ℓ, which can be approximated by $\chi = (1 + \xi_o/\ell)^{-1}$ within an accuracy of about 20%[26]. ξ_o is the BCS coherence distance. A uniform current is assumed to flow in the x direction and the effect

of the self field generated by the currents is considered negligible,[27] because the transverse dimension of the real bridge region is small compared to both the penetration depth and the coherence length at temperatures near to T_c where the G-L equations are strictly valid. This is a fair description of the immediate vicinity of the bridge region where most of the phase change of the superconducting order parameter occurs.

The one-dimensional G-L equations can be written as follows:

$$- \xi^2 \left[\frac{d^2 f}{d^2 x} - f \left(\frac{d\phi}{dx}\right)^2 \right] - f + f^3 = 0 \tag{7}$$

$$i = \frac{c H_c^{\,2} \xi^2}{\Phi_o} f^2 \frac{d\phi}{dx} , \tag{8}$$

where f (x) and ϕ (x) are the amplitude and phase of the reduced gap parameter, $\Delta/\Delta_o = f(x)e^{i\phi(x)}$, Δ_o is the equilibrium gap parameter, and Φ_o is a flux quantum $\frac{hc}{2e}$.. In terms of the reduced variables $X = x/\xi_A$ and $I = i\Phi_o/(cH_c^{\,2}\,\xi_A)$, we obtain

$$\frac{d^2}{dX^2} f_A - I^2/f_A^{\,3} + f_A - f_A^{\,3} = 0 \quad \text{for } |X| > d \tag{9}$$

$$\gamma \frac{d^2}{dX^2} f_B - I^2/(\gamma f_B^{\,3}) + f_B - f_B^{\,3} = 0 \quad \text{for } |X| < d \tag{10}$$

and

$$\phi_c = 2I\left(\int_o^d \frac{dX}{\gamma f_B^{\,2}} + \int_d^{d+X_c} \frac{dX}{f_A^{\,2}}\right) , \tag{11}$$

where $d = L/(2\xi_A)$. ϕ_c is the total phase change across the bridge and X_c is the cut off distance beyond which negligible phase change occurs. Equations (9) and (10) should be solved with the appropriate boundary conditions at $X = d$ and in this case they reduce to the continuity of Δ and the normal component of $\chi\nabla\Delta$,[28] i.e.,

$$\begin{aligned} f_A(d) &= f_B(d) = f_d \quad ; \quad \phi_A(d) = \phi_B(d) \\ \left.\frac{df_A}{dX}\right|_d &= \gamma \left.\frac{df_B}{dX}\right|_d \quad ; \quad \left.\frac{d\phi_A}{dX}\right|_d = \gamma \left.\frac{d\phi_B}{dX}\right|_d \end{aligned} \tag{12}$$

Solutions for these equations with boundary conditions obtained,[23] and those for a particular set of parameters chosen as an example are shown in Fig. 4. The two different types of solutions can be associated with the two different phase relations possible for a given current as shown in the current-phase plot of Fig. 5. Full curves in Fig. 5 correspond to the cutoff distance $X_c = 0$, in Eq. (11) and dotted curves correspond to $X_c = 1$. We notice that for a short bridge a well-defined single valued, odd, periodic current phase relationship (which implies ideal weak link behavior) is achieved, while for a long bridge this relationship is not realizable. Actually, for the long bridge, the solution near $\phi = \pi$ is unstable,

which can be associated with a saddle point of the G-L free energy functional, and the corresponding solution of order parameter shows a dip of width 2ξ well localized inside the bridge.[29]

Critical currents were obtained by looking for the solutions corresponding to maximum I which can be matched at the boundary. Before proceeding to the discussion of the experimental results, let us briefly review the theory of critical current density in small superconductors.

B. Critical Current Density in Superconductors

The amount of free energy density increase F_I associated with the current flow in a superconductor can be expressed as[30]

$$F_I = \int_0^{v_s} W_s(v_s') \, dv_s' \quad , \tag{13}$$

where W_s is the mass current density and v_s is the velocity of the superfluid. When v_s is small, the equilibrium density W_s is proportional to v_s, and their ratio is the density ρ_s of the superfluid in the two fluid model.[31] Hence F_s can be written

$$F_s = F_{so}(\Delta) + \frac{1}{2} \rho_s(\Delta) \, v_s^2 \quad , \tag{14}$$

where F_s is the free energy in the presence of the current and $F_{so}(\Delta)$ is that in the absence of the current. ρ_s is assumed to be dependent only on the gap parameter Δ. Transition to the normal state will occur when

$F_s - F_n = 0$. Suppose that the gap parameter Δ remains constant up to the transition; then the free energy difference $F_n - F_{so}$ is simply the condensation energy $\frac{H_c^2}{8\pi}$, and a transition occurs when

$$\frac{1}{2}\rho_s v_c^2 = \frac{1}{8\pi} H_c^2 , \tag{15}$$

where v_c is the critical velocity. Assuming the temperature dependence $H_c(t) = H_c(0)(1-t^2)$, $n_s(t) = n_s(0)(1-t^4)$ of the two fluid model, with $t = T/T_c$ the reduced temperature, we have for the temperature dependent critical current density

$$I_c(t) = I_c(0)(1-t^2)^{3/2}(1+t^2)^{1/2} . \tag{16}$$

$I_c(0) = \frac{cH_c(0)}{4\pi\lambda_L(0)}$ is the critical current density at $T = 0°K$, $\lambda_L(0)$ being the London penetration depth at 0°K and c the speed of light.

Bardeen has derived the critical current density using a free energy expression based on the model of Bardeen, Cooper and Schrieffer[32] and the superfluid density $\rho_s(\Delta)$ calculated by Miller in the dirty limit.[33] Such a calculation as done by Rogers[34] is shown as the lower broken curve of Figs. 6 and 7. A useful approximation for this curve is given by

$$I_c(t) = \frac{1}{2} H_c(0) \left(\frac{\Delta(0)\sigma}{\hbar}\right)^{1/2} (1-t^2)^{3/2} , \tag{17}$$

where $\sigma = ne^2\ell/mv_F$ is the normal state conductivity of the material, ℓ being the mean free path and v_F being the Fermi velocity of the electrons. Compared to the middle solid curve of Figs. 6 and 7 given by Eq. (16), Bardeen's solution always lies lower than that of two fluid model because of the depression of the gap parameter due to the energy associated with the current flow.

Another expression for the critical current density can be obtained from the Ginzburg-Landau theory,[2] which gives the relation[30]

$$I_c(t) = \frac{e}{m}\left(\frac{2}{3}\right)^{3/2}\left(\frac{H_c^{\,2}\,\rho_s}{4\pi}\right)^{1/2} \tag{18}$$

In G-L regime H_c and ρ_s both vary like (1-t), therefore $I_c(t) \simeq (1-t)^{3/2}$.

At high temperature these expressions have almost the same temperature dependences; $(1-t)^{3/2}$.

C. Experimental Results and Discussions

1. Temperature Dependence of the Critical Current

a. Experimental results. Temperature dependence of the critical current was measured by varying the properties of the bridges in three different ways.

Figure 6 shows how the temperature dependence makes a continuous transition from that of the bulk superconductor (middle curve) toward that of a weak link when the film thickness was changed from 490Å to 2980Å. The thicker films were evaporated onto room temperature substrates and the thinner films onto LN_2 cooled substrates. Otherwise,

all the other experimental conditions were kept nearly the same. Later measurements on the thick film bridges (> 2000Å) deposited onto LN_2 cooled substrates showed no discrepancies from the temperature dependences shown in Fig. 6. Film thicknesses were measured individually even on different films produced during the same evaporation cycle.

Figure 7 shows that similar behavior was observed when the In content of the Sn film was varied, thereby changing the mean free path by impurity rather than size effects. The maximum In concentration was estimated to be less than 3%. For the two short mean free path cases, the film thicknesses were more than twice the estimated mean free path at 4.2°K as listed in the figure. RRR were measured on each bridge sample, and the average value was taken after two or three complete liquid helium to room temperature cycles. The RRR for pure Sn films thicker than 2000Å (which was the case with sample 90A) was typically larger than 25. The mean free path for Sn at T = 300°K was derived from measurements of the anomalous skin effect[35] and was taken to be ℓ_{300} = 94Å.

The temperature dependence curves in Fig. 6 and Fig. 7 are, from bottom to top respectively: Rogers' calculation[34] based on the microscopic theory of BCS; the results of the simple two fluid model; and the temperature dependence of the critical current of an ideal Josephson tunnel junction.[36] In order to clarify Fig. 6 and Fig. 7, the data were normalized at the lowest temperature to the value given by two fluid model.

In Fig. 8, data are shown for the bridges of minimum and maximum length near the transition temperature T_c. The upper theoretical curve is for the tunnel junction model, while the lower one is for the two fluid model. The data on the upper curve were normalized to the theory at a point near t = 0.96, while those on the lower curve were normalized to the two fluid model at the lowest temperatures. Low temperature data for the long bridge is not shown because it was too irregular, probably because the transition took place at several different sites along the bridge.

b. Discussion of experimental results. The three different experiments shown in Fig. 6, 7, and 8 were done with one common objective; namely, to investigate whether there is an enhancement of the supercurrent when the two superconductors on the either side of the bridge are brought closer together, i.e. within a characteristic coherence length. Earlier experiments on very long bridges[37] (~540μ) exhibited the temperature dependence derived for bulk-like behavior from the two fluid model. Our observations on bridges shorter than 0.5μ (which, incidentally showed very pronounced ac Josephson effect near T_c) always had a temperature dependence of the critical current linear in $(T_c - T)$ at high temperatures. The same dependence has also been observed in a 'ruptured' tunnel junction experiment.[38] The most interesting fact is that the large amount of critical current in excess of the value which the microbridge would have if it behaved according to the bulk dependence is a prerequisite for a strong ac Josephson effect. Josephson[6] and Anderson[39] have stressed that the existence of the coupling energy, which is dependent on the phase differences of the two bulk superconductors on

either side of the weak link, is the most important parameter for ac Josephson interference effects. This phase dependent coupling energy couples the superconductors into a coherent state, which enables a supercurrent to flow between them due to the canonical commutation relation between the number and phase. In the tunnel junction, the tunneling transition matrix elements are of the order $e^{-k_F \ell}$, where the Fermi wave vector $k_F \sim 10^8$ cm^{-1} and ℓ is the thickness of the barrier. Therefore, when ℓ is much larger than a few tens of an angstroms the coupling is negligible and thermal fluctuations destroy the coherence. Increased coupling vestures the phase coherence so that there is a finite supercurrent flowing when ℓ is reduced. However, finite amount of supercurrent always flows through a microbridge (up to the critical current of the material) no matter how long the bridge is. As the temperature is raised near T_c, this intrinsic bulk critical current is reduced (for instance at t=0.95 it is 4% of the low temperature value), while the effective distance between the two superconductors across the weak link is reduced because the temperature dependent coherence length of the outside superconductor increases. Because of the presence of a strong superconductor, which has a coherence length longer than the characteristic dimensions of the bridge, the supercurrent carrying capacity of the bridge is enhanced. The amount of enhancement of the supercurrent of the microbridge above its bulk behavior can thus be considered to be a measure of the strength of the Josephson-junction like effect. Furthermore, the relative ratio of this enhancement over the bulk value should be large to minimize the bulk like effect, which tends

to obscure any coherent phase difference set up inside the superconductor. This is the reason why the true Josephson effect can be seen only near T_c on the microbridges.

This qualitative argument can be seen more clearly through the one-dimensional model discussed in III.A. Before we embark on the discussion of the solution of Baratoff et al., let us calculate the coherence length of the samples shown in Fig. 6 and 7. The Ginzburg-Landau coherence length can be written as

$$\xi(T) = 0.74\, \xi_o \left(\frac{T_c}{T_c - T}\right)^{1/2} \quad \text{pure metal}$$

$$\xi(T) = 0.85 \left(\frac{\xi_o \ell\, T_c}{T_c - T}\right)^{1/2} \quad \text{dirty metal}\ , \tag{19}$$

where BCS coherence distance $\xi_o = 0.18 \frac{\hbar v_F}{k_B T_c}$ for Sn is 2300Å.

The mean free path ℓ is taken to be the film thickness d following Millstein and Tinkham[40] rather than $\frac{8d}{3}$ as given in standary textbooks.[35] The upper two curves in Figs. 6 and 7 were taken to be pure and the lower two dirty. In Table 1 we give the value of ξ at reduced temperature t = 0.9 and 0.95. Typical bridge length as determined by the electron microscope was ~6000Å. Both samples shown in Fig. 8 were in the pure limit. Note that $J_c \propto (T_c - T)$ whenever $L \lesssim \xi$, while $J_c \propto (T_c - T)^{3/2}$ when $L > 2\xi$. Even for the long bridge some enhancement is expected very close to T_c, but in that situation the critical current is becoming too small to see the effect. G-L theory is exact only wear T_c and the calculated ξ at t = 0.9 are estimated to be a little larger than the actual value.

Let us now consider a semiquantitative explanation based on the model of Baratoff et al. We will examine the two extreme cases: linear dependence and bulk behavior. Let us go back to Fig. 4. Of the two solutions shown, the one labeled by f_{01} is not possible with a constant current biased circuit, because this corresponds to the region where $\frac{dJ}{d\phi} < 0$ in Fig. 5; the other branch however is physically realizable. Let us consider a bridge of length $L < \xi$ so that the boundary between superconductor and the bridge is at the distance $d < 0.5$ in Fig. 4. Since the superconducting gap parameter does not change appreciably within a coherence length, and remembering that since the strong superconductors are on both sides the slope of the gap parameter should be zero at the middle of the bridge, it is readily seen that the depression of gap parameter in the bridge is very small. In this case we can write the current at the boundary X = d

$$i = \frac{c}{\Phi_o} H_c^{\,2}(T)\, \xi^2(T)\, f^2 \left.\frac{d\phi}{dx}\right|_{x=d} \propto (T_c - T) \left.\frac{d\phi}{dx}\right|_{x=d}$$

We have used the temperature dependence of $H_c(T) \propto (T_c - T)$ and $\xi(T) \propto (T_c - T)^{-1/2}$ and assumed f=1 at X=d. The critical current is reached when the total phase change across the bridge is about $\frac{1}{2}\pi$ as shown in Fig. 5. In the light of our experimental results the distance over which the phase change occurs is held constant in this high temperature region. Therefore, $\frac{d\phi}{dx}$ at the critical current is constant.

In the other limit, bulk behavior, our data closely follows the predictions of the two fluid model at low temperature rather than that of the microscopic theory.[30] This can be explained in the light of the model of Baratoff et al. The microscopic theory was based on the assumption that the transition to a normal state takes place uniformly over the total volume considered, but in the real experimental situation the development of a local hot spot of the dimension of the coherence length initiates the appearance of a measurable voltage across the sample. This is the case with our experiment because the center of the bridge region is not many coherence lengths away from the strong superconductor even at the lowest temperature, (ξ_o ~2300Å and bridge length ~6000Å). Therefore, marked depression of the order parameter does not occur at the critical current. In the light of this argument, our data were all normalized to the two fluid model at low temperature as stated in the previous section.

The drop of data points below the linear dependence (a) of Fig. 8 is due to the noise effect which is dominant near T_c when the coupling of the bridge $E_c/k_B = \phi_o \frac{J_c}{2\pi k_B}$ is comparable to the noise temperature. The decrease was initiated at J_c ~100μA, corresponding to a noise temperature somewhat higher than room temperature, but this is not unreasonable considering that non-thermal noise sources are present which will contribute to the decoupling and will contribute to the estimation of an effective noise temperature.

Because of the uncertainties of the shape of the bridge region, the estimate of the cross-sectional area is subject to large error. Taking the thickness of the bridge to be twice that of the film while using the width measured by optical microscope, the critical current density at the lowest temperature ($< 1^{\circ}K$) was within the range of 0.8 $0.8 \sim 2 \times 10^7$ A/cm^2 which is in good agreement with previous measurements.[37,41]

c. Penetration depth correction. The most significant error that can be introduced by taking the critical current given in Figs. 6 and 7 as the critical current density arises from non-uniform current distribution across the cross section of the bridge area when the penetration depth is comparable to or smaller than the transverse dimension of the bridge. As mentioned in II.A., the thickness of the bridge is about twice the film thickness because of the piling up of Sn along the scratch path. The London equation has not been exactly solved for the two dimensional rectangular cylinder case. Cooper[42] has discussed the problem qualitatively and Marcus[43] has given approximate solution together with numerical results for the case when one side is 10 times longer than the other side. We have made the rather crude assumption that our bridge can be approximated by transforming it into a circular cylinder of the same area as the rectangle, which lets us use the known exact solutions. The penetration depth for Sn is taken from Miller.[33] The mean free path in the bridge region is taken to be the radius of the cylinder rather than the diameter, as transformed from the rectangle on the equal area basis. Then the formula by which the measured critical current should be multiplied to get a

true critical current density is given by $\frac{R}{2\lambda} \frac{I_0(R/\lambda)}{I_1(R/\lambda)}$, where R is the radius and λ is the penetration depth and I_0, I_1 are the modified Bessel functions, and is shown in Fig. 9. This correction is as large as 50% for 2000Å thick films at low temperature and is even larger for 3000Å thick films, but is less than 5% for 500Å thick film at all temperatures. At high temperature ($t > .9$), the correction is less than 10% even for the thickest films. As the correction is small, we may safely neglect the error due to the cylindrical transformation. The above correction is much overestimated. First, our films have usually rough surface structure which gives shorter mean free path, hence longer penetration depth. Longer penetration depth was actually observed on the rough Sn films.[44]

Secondly, considering that the correction formula predicts a big difference between 2000Å thick films and 3000Å thick films, while the experimental data have almost the same temperature dependences, the actual penetration depth is estimated to be much longer than the theoretical value. In view of these arguments the correction formula given above may be considered as an upper limit for the penetration depth corrections.

2. Magnetic Field Dependence of the Critical Currents

a. Critical current of single bridge. In all cases, magnetic fields on the order of a few gauss parallel to the film plane had no effects on the I-V characteristic of the bridge. The bridge was, however, very sensitive to the perpendicular field, because the thin superconducting film in the perpendicular field behaves like a type II[45]

superconductor. H_{c_1} associated with the film is very small because of the demagnetization factor of the film geometry. In fact, in measuring the critical current, care must be taken to eliminate the asymmetry in the I-V characteristics. Critical current was easily modulated within 5% of the total value in a rather irregular fashion, and this effect was pronounced at low temperatures. It was indeed difficult to make a perfectly symmetric bridge with scratching techniques. If the flux is trapped inside the bridge (which has geometrical asymmetry), it is quite probable that this will interfere with the bias current in an asymmetrical way, adding in one direction and subracting in the other direction. Figure 10 shows the two experiments done with the perpendicular field. The upper data show that the critical current has two bumps, which can be associated with fluxoid moving in and out of the bridge as we increase the field. On the larger scale, however it slowly decreases until it comes to a point where the I-V characteristic, as shown in the insert, makes a smooth, rounded transition from the zero voltage line. We associate this point with the start of the fluxiod movement in the large patches of film on either side of the bridge. Up to this field, the I-V curve shows a sharp transition i.e., it departs from zero voltage with a finite slope. The sharp break in the curve is still seen at finite voltage which is an indication of the sudden voltage development across the bridge.

The lower data taken at higher temperature show essentially the same results except for the absence of the irregular bumps. The physical explanation is as follows: At this temperature the minimum

size of the fluxoid is too big to fit in the bridge.

If we assume a fluxoid containing one single flux quantum, the condition that the circulating associated with this current flux line should not exceed the critical current imposes a lower limit on the diameter that the fluxoid can have which this is inversely proportional to I_c. The critical current for the upper data was 0.5 mA and that for the lower data was 0.1 mA.

b. Critical current modulation of double bridge. To complete the investigation of the quantum interference effects of the microbridge, we have done a critical current modulation experimenta on the double bridge as schematically shown in the insert of Fig. 11. Theoretical analyses of the double bridge in the most general case can be found elsewhere,[46] and elegant experiments have been done by Fulton and Dynes[47]

Our bridge was made by double-scratching the film. The critical current was measured on an oscilloscope while manually varying the applied magnetic field. The data shown in Fig. 11 were the best in the narrow sense that they conform to the theoretically predicted curve. Measurements were done at rather lower temperature to facilitate the observation on the oscilloscope. The modulation depth of ~200μA was very large compared to the typical value of 1μA observed on the double bridge using other kind of weak links. The loop inductance was calculated for the typical geometry used in our experiment, 10^{-6} m wide, 2.5×10^{-3} m long, with the current distribution given by Edwards and Newhouse[48] and was about $\sim 2 \times 10^{-11}$ henry, which agrees will with the modulation depth observed.

One intrinsic problem with this interferometer was that the magnetic field must be applied perpendicular to the film plane, thereby inducing a type II behavior in the film. Irreversibility and irregularities associated with the most of these experiments most probably arise from the trapped flux in the films. This behavior is quite complex as it depends upon the history of the applied magnetic field and is not generally reproducible in any way.

IV. CURRENT VOLTAGE CHARACTERISTICS AT FINITE VOLTAGE

We will separate our discussion into the two different experimental cases at finite voltage: Undriven mode is the case without any external synchronizing signal applied to the bridge and driven mode is the case when external high frequency ac signal is applied to the bridge, thereby producing an ac interference effect.

A. Undriven Mode

The lumped circuit parameter model for the superconducting weak link as proposed by McCumber[49] and Stewart,[50] and recently studied experimentally by Hansma et al.[51] is a powerful tool with which to study the finite voltage region of the weak link in the absence of an adequate microscopic model. A lumped circuit parameter model is shown in Fig. 12(a). It is a current biased circuit and is different from the model of McCumber and of Stewart in that it has an inductance L in series with the microbridge. Distributed capacitance and distributed conductance were lumped as a shunt capacitance C and shunt conductance G. The inductance L may be best illustrated by considering the energy E associated with an electric current carried by particles of mass m and number density n.[52]

$$E = \int 1/2\ \mu H^2 d\underset{\sim}{r} + \int 1/2\ mv^2\ d\underset{\sim}{r} \tag{20}$$

For a homogeneous conductor of uniform cross section and uniform current distribution, Eq. (20) can be written

$$E = 1/2\ L_M I^2 + 1/2\ [(m/ne^2)\ (\ell/\sigma)]I^2 \qquad (21)$$

where L_M is the usual magnetic inductance, and $L_k = (m/ne^2)\cdot(\ell/\sigma)$ is the kinetic inductance, ℓ and σ being the length and cross-sectional area of the bridge, respectively. The second term becomes important when ℓ/σ is large as it is in our bridge. For a typical bridge 10^{-6} m long and 10^{-13} m^2 area, $L_k \sim 10^{-13}$ Henry while L_M is about half of L_k.

For a voltage of 0.1 mv across the bridge, the Josephson frequency $\frac{2eV}{h} \approx 5 \times 10^{10}$ Hz and the inductive impedance associated with this frequency is about 0.03 Ω, which is comparable to the actual resistance of the bridge. Such an inductance is important in our long, narrow superconducting strips, and has been measured experimentally.[44,53]

The total current $I_{dc}(t)$ is the sum of the current $C\ \frac{dV(t)}{dt}$ flowing through the capacitance, the current $GV(t)$ through the conductance and the pair current $I_c \sin \phi(t)$ through the combination of the inductance L and the ideal bare bridge which has an ideal Josephson current-phase relationship. L is put in direct series with the Josephson junction because the effect of L is important only at high frequencies corresponding to the Josephson current.

The equation describing the circuit of Fig. 12(a) can be written

$$I_{dc}(t) = C\ \frac{dV}{dt} + GV + I_c \sin \phi \quad . \qquad (22)$$

Using the Josephson frequency-voltage relation

$$\frac{d\phi}{dt} = \frac{2eV'}{\hbar} \tag{23}$$

where V' is the voltage across the bare Josephson junction, and the voltage drop across L is $-LI_c(\cos\phi)\dot{\phi}$, we can rewrite Eq. (22) in terms of reduced variables,

$$\alpha(\theta) = \beta_c \frac{d}{d\theta}\left(\frac{d}{d\theta}\phi - \beta_c \frac{G^2L}{C}\cos\phi\frac{d\phi}{d\theta}\right)$$

$$+ \left(\frac{d}{d\theta}\phi - \beta_c \frac{G^2L}{C}\cos\phi\frac{d\phi}{d\theta}\right) + \sin\phi , \tag{24}$$

using a normalized current $\alpha(\theta) = I_{dc}(t)/I_c$, a dimensionless time variable $\theta = 2eI_c t/\hbar G$, and a dimensionless admittance ratio $\beta c = 2eI_c C/\hbar G^2$. This highly non-linear equation will be discussed for two cases in conjunction with our experiments.

Figures 13 and 14 show the current voltage characteristics of microbridges at different temperatures. These two figs. represent the two extreme cases of the microbridges tested in our experiments. Figure 13 corresponds to the case of low conductance, long bridge, i.e., bridge length L longer than the coherence length $\xi(T)$ at all temperatures. For this category of bridges, the ac Josephson effect was always minimal and the temperature dependence of the critical current was fitted very well be the bulk formula. Figure 14 shows the case of a high conductance, short bridge, where $L \sim \xi(T)$ at low temperature and $L \ll \xi(T)$ at high temperature. For this kind of bridge, a pronounced ac Josephson effect

was observed and the temperature dependence of the critical current followed the linear (T_c-T) law at high temperature.

Figure 13(a) shows the low temperature data. Because of the low conductance and high critical current of this sample, the voltage jump at the transition is about 6mV, which is rather high compared to the usual value, and the upward curvature of the I-V characteristic shows the importance of the inductive term in this region. The ac current across the inductance contributes a finite dc voltage here due to the non-uniform time-variation of the phase in current biased bridges.[54] As the current is reduced, the voltage and therefore the Josephson frequency are decreased. The contribution from the inductive term then gradually diminishes until the bias point moves down to the 'hump' and a transition is made to a different regime, shown as a broken convex curve, which we shall call the capacitive region. In Fig. 13(b), the critical current has decreased, as has the voltage associated with the transition, moving the inductive region toward larger values of normalized voltage: here, where the reduced temperature $t \sim 0.9$, the characteristic is primarily capactive for all $GV/I_c < 1$, and amount of hysteresis is reduced to about half of the low temperature value. In Fig. 13(c), where $t \sim 0.95$, the hysteresis is gone and the transition is reversible. In Fig. 13(d), only 30 millidegrees from the transition, the finite voltage region joins smoothly to the critical current because the coupling energy of the bridge is comparable to the equivalent noise energy.

In Fig. 14(a), the voltage at transition is about 1 mV and the inductance is smaller than that of Fig. 13 because of the shorter length of the bridge. The characteristics are all capacitive for $GV/I_c < 1$. In Fig 14(b), where $t \sim 0.84$, the temperature has been raised and the critical current reduced; the hysteresis becomes smaller and the finite voltage region tends more or less to a straight line. In Fig. 14(c) where $t \sim 0.97$, we observe two quite distinct regions. The initial transition is very sharp (with finite slope) and the finite voltage region has a higher conductance of a given V than at the lower temperature. As the current is increased above 1.1 I_c, the bridge goes reversibly into a region exhibiting the low temperature conductance. In Fig. 14(d), the finite voltage region shows about the same conductance as the low current conductance in (c). The physical reasoning is that in (c), where $t \sim 0.97$, the effective length of the bridge is shorter at the transition than it was at lower temperature because of the increased coherence length of the strong superconductors outside. A slight increase above the critical current disturbs this situation and restores the length to its original low temperature value. The fact that, (1) the transition is very sharp, and (2) the coupling energy corresponds to a noise temperature of $\sim 10^4$ °K, show that this phenomenon is not due to noise. The fact that the initial conductance of (c) is exhibited by (d) implies there is minimum finite effective length of the bridge no matter how strong the enhancement of coherence length is. This is precisely the assumption we used in discussing the linear temperature dependence of the critical current in the previous section.

There were some difficulties in determining the asymptotic slope of the I-V curve because of the transition to inductive behavior at high current (high voltage); we took the average slope between $t \sim 0.25$ and $t \sim 0.7$ (where there is little variation with the temperature) to be the correct value.

Since the effect of inductance is usually not important when $V \to 0$, it is relevant to compare the dependence of the hysteresis on the admittance ratio to McCumber's model. This model predicts that the hysteresis is dependent on both the capacitance and the critical current. In effect, the energy $1/2\ CV^2$ associated with the capacitance C at finite voltage is a measure of the stiffness keeping the bridge at finite voltage, while the coupling energy $\phi_o \frac{I_c}{2\pi}$ is a measure of the pull into the zero voltage region. The ratio of these two energies is given by the admittance ratio β. Figure 15 shows the dependence of the hysteresis, α_{cutoff}, on β for the two samples whose I-V curves were discussed in Fig. 13 and 14. The data were normalized at the point which gave best fit for the overall range of temperature. Capacitances as estimated from the fitting were 5 pf and 57 pf for sample 71 B and 22 C respectively.

There was one discrepancy between the theory of McCumber and that of Stewart; whether the transition from a finite voltage to the zero voltage is continuous or not. In our experimental situation the transition was always discontinuous. However, assuming that a discontinuous transition occurs when the noise energy kT_n just equals the electrostatic energy $1/2\ CV^2$, we obtain a reasonable noise temperature of 600°K for our system.

B. Driven Mode

The most effective way of studying ac Josephson effects is to apply an external ac signal to the junction to produce the synchronization effect first suggested by Josephson[6] and later applied by Shapiro to tunnel junctions.[55] This produces singularities in the I-V characteristic at voltages defined by the relation

$$n\hbar\omega = m\,(2eV)$$

where n and m are integers, V is the dc voltage across the Josephson junction, and ω is the angular frequency of the applied signal. In the case of the current-biased junction, these singularities appear as current steps at constant voltage. Figure 16 shows such an I-V characteristic. Good agreement between experimental data and the theoretical Bessel function dependence of the induced current step heights on applied field have been achieved for tunnel junctions.[56]

This ac Josephson effect has been observed in many other types of weak links, such as S-N-S, point contact and Dayem bridges, but the field dependence of the induced current step height is usually not in good agreement with the Bessel function behavior.[57] Our microbridges were also used to study the field dependence of the current step heights, as well as the orientation dependence of the bridge response to the applied field.

A strong ac Josephson effect, as shown in Fig. 16, was observed whenever $L \ll \xi(T)$, where L is the bridge length and $\xi(T)$ is the coherence length. The explanation of why the enhancement of the critical current over its bulk value is necessary for the ac Josephson effect to occur was given in III.

The experimental evidence of this criterion, $L \ll \xi(T)$, was discussed in III and IV, and was indicated by a linear temperature dependence of the critical current and the I-V characteristics as shown in (c) and (d) of Fig. 14. The microwave electric field was always parallel to the bridge in this case, as a slight deviation from parallel field reduced the effect markedly. Dependence of the current step heights on the field is shown in Fig. 18, and will be discussed later.

The type of response shown in Fig. 17 occurred in many different situations where the criterion $L \ll \xi(T)$ was not fulfilled (as in the long bridge at high temperature or the short bridge at very low temperature) when a good coupling of microwave field to the bridge was achieved. We associate this regime with synchronized flux flow[58] since the experimental data shown in Figs. 16 and 18 are in very good agreement with junction-like behavior based on Josephson's current-phase relationship, while Fig. 17 is not.

In determining the microwave power dependence of the step heights, we must decide whether the applied field can be considered as a current source or a voltage source. Waldram et al.[54] showed that an ideal tunnel junction sees an effective voltage source because of its high shunt capacitance, while other weak links (with low capacitance) see an effective current source. A simple Bessel function dependence is expected only for a voltage source. Our microbridges see an effective source, since their impedance is 100m Ω at most, and their shunt capacitance is ~10 pF, while the characteristic impedance of the X-band wave guide used in our experiment is ~500 Ω.

Calculations based on the lumped circuit parameter model as shown in Fig. 12(b) using an ac current source and Josephson's relations have recently been published.[59,60] The equation for the circuit is

$$I_{dc}(t) + I_{rf} \cos \omega t = \frac{G}{2e} \frac{d\phi}{dt} + I_c \sin \phi \qquad (24)$$

Figure 18 shows the fitting of our data to the solution given by Russer[59] for the parameter $\xi = \frac{\hbar\omega G}{2eI_c} = 0.1$. Our experimental ξ was 0.12. The microwave power was normalized at the first zero of the n=0 step, and the step height was normalized to give the best fit to the linearly decreasing portion of the n=0 curve just below the first zero. Because of this good agreement with the theoretical value, we conclude that Josephson's junction-like relation is correct for the microbridge in this regime near $T=T_c$.

The initial increase of the n=0 step with power is the so-called Dayem effect[11,61] which is not clearly understood. It was proposed recently[24] that this enhancement is due to the restoration of the critical current to its maximum value from the reduced one as the fluctuations of the phase difference across the bridge are suppressed by the rf signal. In Fig. 18, we show an n=0 enhancement of about 100μA, which is a typical value observed during our experiments. This value, corresponding to noise temperature of 3000°K, is rather larger than that can be associated with room temperature noise, and somewhat larger than the effective noise temperatures estimated from other behavior in the previous sections.

V. SUMMARY AND CONCLUSIONS

The most important result of our experiment is the determination that the ratio of the coherence length $\xi(T)$ to the actual length of the bridge L is the parameter governing whether the bridge behaves like a bulk superconductor or like a Josephson junction. We have shown that Josephson-junction like behavior can be observed only near T_c, where the enhancement of critical current due to the increased coherence length of the strong superconductor on either side of the bridge exceeds the intrinsic critical current of the bulk. When $L \ll \xi(T)$, and near T_c, the bridges had a linear temperature dependence of the critical current, $I_c \propto (1-t)$, and exhibited strong ac interference effects. The experimental data on induced step heights versus applied microwave dield were in excellent agreement with theory, based on the lumped circuit parameter model of Fig. 12(b) and Josephson's sinusoidal current-phase relationship (and his voltage-frequency relationship). In this limit, we conclude the bridge behaves as a proper Josephson junction following the usual Josephson relation.

When $L \gg \xi(T)$, the temperature dependence of the critical current is given by bulk formula, $I_c \propto (1-t^2)^{3/2}\,(1+t^2)^{1/2}$, of the two fluid model, and the bridge showed rather complicated ac interference effects at high temperature. We associate this limit with bulk behavior. The continuous transitions from bulk behavior to Josephson-junction like behavior seen in the temperature dependence of the critical current were achieved by continuously varying the size and impurity dependent coherence length from $\xi \ll L$ to $\xi \gg L$. Baratoff et al.'s[23] one-dimensional model of a weak link adequately explains the experimental

results for the critical current, and provides a theoretical justification for assuming a sinusoidal current-phase relationship in short bridges.

We have also experimentally demonstrated that there is a temperature above which the diameter of the fluxoid containing one flux quantum is too big to fit inside the bridge. Our observation of microwave induced steps above this temperature shows that flux flow can not be the sole physical mechanism underlying the finite voltage behavior of microbridges near T_c.

The current-voltage characteristics and hysteresis parameters, when analyzed by a slightly modified version of the lumped circuit model of McCumber[49] and Stewart,[50] were in satisfactory agreement with the theory, especially at high temperature where the bridges were in the junction-like regime.

Table I. High Temperature Coherence Length (Fig. 6)

Sample	Thickness (Å)	ξ (0.9)(Å)	ξ (0.95) (Å)
34B	2980	5382	7611
22C	1900	5382	7611
55C	800	3645	5154
71B	490	2853	4034

Table II. High Temperature Coherence Length (Fig. 7)

Sample	Mean free path (Å)	ξ (0.9) (Å)	ξ (0.95) (Å)
90A	-	5382	7611
85A	2100	5382	7611
87A	658	3306	4675
93A	405	2594	3668

Footnote: Typical bridge length was ~6000Å.

ACKNOWLEDGEMENTS

I would like to thank Professor G. I. Rochlin for his invaluable support and guidance during the course of this work. I would like to thank Professor M. L. Cohen and Professor S. N. Kaplan for their advice and encouragement which were most welcome at the time when I had to make a decision on my change of career from engineering to physics, and for their constant guidance thereafter. I would like to thank Professor J. Clarke for valuable discussions on many aspects of the superconducting weak links.

At last, and most especially, I would like to thank my wife, Agnes, for her continued support and encouragement throughout the long periods of my graduate studentship.

This work was done under the auspices of the United States Atomic Energy Commission.

REFERENCES

1. F. London, Proc. Roy. Soc. (London) A 152, 24 (1935); Phys. Rev. 74, 562 (1948).

2. V. L. Ginzburg and L. D. Landau, Zh. Eksp. Teor. Fiz. 20, 1064 (1950) (English translation in Men of Physics: L. D. Landau I by D. ter Haar, Pergamon Press, Oxford, 1965).

3. L. P. Gor'kov, Zh. Eksp. Teor. Fiz. 36, 1918 (1959) [Sov. Phys.-JETP 9, 1364 (1959)].

4. B. D. Josephson, Phys. Letters 1, 251 (1962).

5. B. D. Josephson, in Superconductivity Vol. 1, edited by R. D. Parks (Marcel Dekker, New York, 1969).

6. B. D. Josephson, Advan. Phys. 14, 419 (1965).

7. P. W. Anderson and J. M. Rowell, Phys. Rev. Letters 10, 230 (1963).

8. J. Clarke, Proc. Roy. Soc. (London) A 308, 447 (1969).

9. J. E. Zimmerman and A. H. Silver, Phys. Letters 10, 47 (1964); Phys. Rev. 141, 367 (1966).

10. P. W. Anderson and A. H. Dayem, Phys. Rev. Letters 13, 195 (1964).

11. A. H. Dayem and J. J. Wiegand, Phys. Rev. 155, 419 (1967).

12. P. E. Gregers-Hansen and M. T. Levinsen, Phys. Rev. Letters 27, 847 (1971).

13. R. Hultgren et al. Selected values of thermodynamic properties of metals and alloys (John Wiley, New York, 1963).

14. A. B. Pippard, Proc. Roy. Soc. (London) A 216, 547 (1953).

15. T. Aomine, H. Abe and Y. Shibuya, J. Phys. Soc. Japan 20, 282 (1965)

16. G. I. Rochlin, Rev. Sci. Instr. 41, 73 (1970).

17. This standard thermometer was calibrated at N. E. Phillips' Laboratory, Department of Chemistry, U. C., Berkeley.

18. G. Cataland and H. H. Plumb, J. Res. Natl. Bur. Std. (U.S.) 70A, 243 (1966).

19. C. G. Montgomery ed., Technique of microwave measurements Vol. 1 (McGraw-Hill, New York, 1947) RLS-11.

20. P. J. Hart, Universal tables for magnetic fields of filamentary and distributed circular currents. (American Elsevier, New York, 1967).

21. M. H. Cohen, L. M. Falicov, and J. C. Phillips, Phys. Rev. Letters 8, 316 (1962).

22. See for instance, G. Deutscher and P. G. de Gennes, in Superconductivity Vol. 2, edited by R. D. Parks (Marcel Dekker, New York, 1969).

23. A. Baratoff, J. A. Blackburn and B.B. Schwartz, Phys. Rev. Letters 25, 1096 (1970).

24. P. V. Christiansen, E. B. Hansen, and C. J. Sjöström, J. Low Temp. Phys. 4, 349 (1971).

25. L. P. Gor'kov, Zh. Eksp. Teor. Fiz. 37, 1407 (1959) [Sov. Phys. - JETP 10, 998 (1960)].

26. D. H. Douglass Jr. and L. M. Falicov, in Progress in low temperature physics, vol. 4, edited by C. J. Gorter (North-Holland Pub. Co., Amsterdam, 1964).

27. J. S. Langer and V. Ambegaokar, Phys. Rev. 164, 498 (1967).

28. R. O. Zaitsev, Zh. Eksp. Teor. Fiz 50, 1055 (1966) [Sov. Phys. JETP 23, 702 (1966)].

29. A. Baratoff, Conference on fluctuations in superconductors, Asilomar, Calif., by W. S. Goree and F. Chiton (Stanford Research Institute, Menlo Park, Calif., 1968).

30. J. Bardeen, Rev. Mod. Phys. 34, 667 (1962).

31. J. Bardeen, Phys. Rev. Letters 1, 339 (1959).

32. J. Bardeen, L. N. Cooper, and J. R. Schrieffer, Phys. Rev. 108, 1175 (1957).

33. P. B. Miller, Phys. Rev. 113, 1209 (1959).

34. K. T. Rogers, Ph.D. Thesis, Univ. of Illinois, 1960 (unpublished).

35. J. L. Olsen, Electron transport in metals (Interscience Publishers, New York, 1962).

36. V. Ambegaokar and A. Baratoff, Phys. Rev. Letters 10, 486 (1963).

37. T. K. Hunt, Phys. Rev. 151, 325 (1966).

38. O. Iwanyshyn, J. D. Leslie and H. J. T. Smith, Can. J. Phys. 48, 470 (1970).

39. P. W. Anderson, in: Lectures on the many-body problem, Ravello 1963, vol. 2, Ed. E. R. Caianello (Academic Press, New York, 1964) and Progress in low temperature physics vol. 5, Ed. C. J. Gorter (North-Holland Co., Amsterdam, 1967).

40. J. Millstein and M. Tinkham, Phys. Rev. 158, 325 (1967).

41. R. E. Glover and H. T. Coffey, Rev. Mod. Phys. 36, 299 (1964).

42. L. Cooper, in Proceedings of the Seventh International Conference on Low Temperature Physics (University of Toronto Press, 1961), p. 416.

43. P. Marcus, Ref. 42, p. 418.

44. R. Meservey and P. M. Tedrow, J. Appl. Phys. 40, 2028 (1969).

45. M. Tinkham, Phys. Rev. 129, 2413 (1963).

46. R. de Bruyn Ouboter and A. Th. A. M. De Wade, in Progress in low temperature physics vol. 6, Ed. by C. J. Gorter (North-Holland Pub. Co., Amsterdam, 1970).

47. Fulton and Dynes, Phys. Rev. Letters 25, 794 (1970).

48. V. L. Newhouse, Applied superconductivity (John Wiley, New York, 1964).

49. D. E. McCumber, J. Appl. Phys. 39, 3113 (1968).

50. W. C. Stewart, Appl. Phys. Letters 12, 277 (1968).

51. P. K. Hansma, J. N. Sweet and G. I. Rochlin, to be published (in print).

52. F. London, Superfluids vol. 1 (John Wiley, New York, 1950).

53. W. A. Little, Proc. of the Symposium on the Physics of Superconducting Devices, Charlettesville, Va. (1967), p. s-1.

54. J. R. Waldram, A. B. Pippard and J. Clarke, Phil. Trans. Roy. Soc. London A 268, 265 (1970).

55. S. Shapiro, Phys. Rev. Letters 11, 80 (1963).

56. S. Shapiro, A. R. Janus and S. Holly, Rev. Mod. Phys. 36, 223 (1964).

57. C. C. Grimes and S. Shapiro, Phys. Rev. 169, 397 (1968).

58. P. L. Richards and P. W. Anderson, Phys. Rev. Letters 14, 540 (1965) and P. W. Anderson, Rev. Mod. Phys. 38, 298 (1966).

59. P. Russer, to be published.

60. H. Fack and V. Kose, J. Appl. Phys. 42, 320 (1971).

61. A. F. G. Wyatt, V. M. Dmitriev, W. S. Moore and F. W. Sheard, Phys. Rev. Letters 16, 1166 (1966).

FIGURE CAPTIONS

Fig. 1. Schematic of the microwave dewar system.

Fig. 2. Block diagram of electronics and microwave system.

Fig. 3. Sketch of bridge and corresponding one-dimensional model.

Fig. 4. Sample solution of one-dimensional model for $d = 1.0$, $\gamma = 0.6$, and $f_\infty^2 = 0.9850$; $f_{01}^2 = 0.9761$, and $f_{02}^2 = 0.0451$. (From Ref. 23)

Fig. 5. Current-phase relationship of a superconducting microbridge for various values of d, as calculated by Baratoff et al. (Private Communication)

Fig. 6. Temperature dependence of the critical current for various film thickness. Upper broken curve is the theoretical calculation of the critical current density for a tunnel junction by Ambegaokar and Baratoff; the middle solid curve is the critical current density of a bulk superconductor calculated by the two fluid model; the lower broken curve is the BCS model.

Fig. 7. Temperature dependence of the critical current of the microbridges for various impurity content of the film. Curves are the same as in Fig. 6.

Fig. 8. Temperature dependence of the critical current at high temperatures for two bridges of different lengths. The upper curve is the calculation for a tunnel junction and the lower curve is that for a bulk superconductor by two fluid model as in Fig. 6.

Fig. 9. Correction factor in converting critical current to critical current density in a cylindrical microbridge.

Fig. 10. Critical current versus perpendicular magnetic field; upper data correspond to when a fluxoid can fit in the bridge, lower data correspond to when a fluxoid is too big to fit in the bridge.

Fig. 11. Critical current modulation of a double bridge by perpendicular magnetic field.

Fig. 12. Lumped circuit parameter model of a microbridge used for a) undriven mode. b) driven mode.

Fig. 13. I-V characteristics of a bridge, whose length L is long compared to the coherence length ξ at all temperature. A bridge of this kind behaves like a bulk superconductor. Abscissae and ordinates are in terms of the normalized voltages and currents.

Fig. 14. I-V characteristics of a bridge, whose length L is short compared to the coherence length at high temperature. A bridge of this kind shows a Josephson junction like behavior at high temperature. Abscissae and ordinates are in terms of the normalized voltages and currents.

Fig. 15. Amount of hysteresis α_{cutoff} versus circuit admittance ratio β for both a long bridge and a short bridge.

Fig. 16. Typical driven I-V characteristic for a bridge which shows a pronounced ac Josephson effect.

Fig. 17. Low temperature driven I-V characteristic of a bridge which had shown a pronounced ac Josephson effect at high temperature. The vertical arrows indicate the every tenth step.

Fig. 18. Field dependence of the microwave induced step height. The solid line is P. Russer's calculation for $\xi = \frac{\hbar\omega G}{2eI_c} = 0.1$, close to our experimental $\xi = 0.12$.

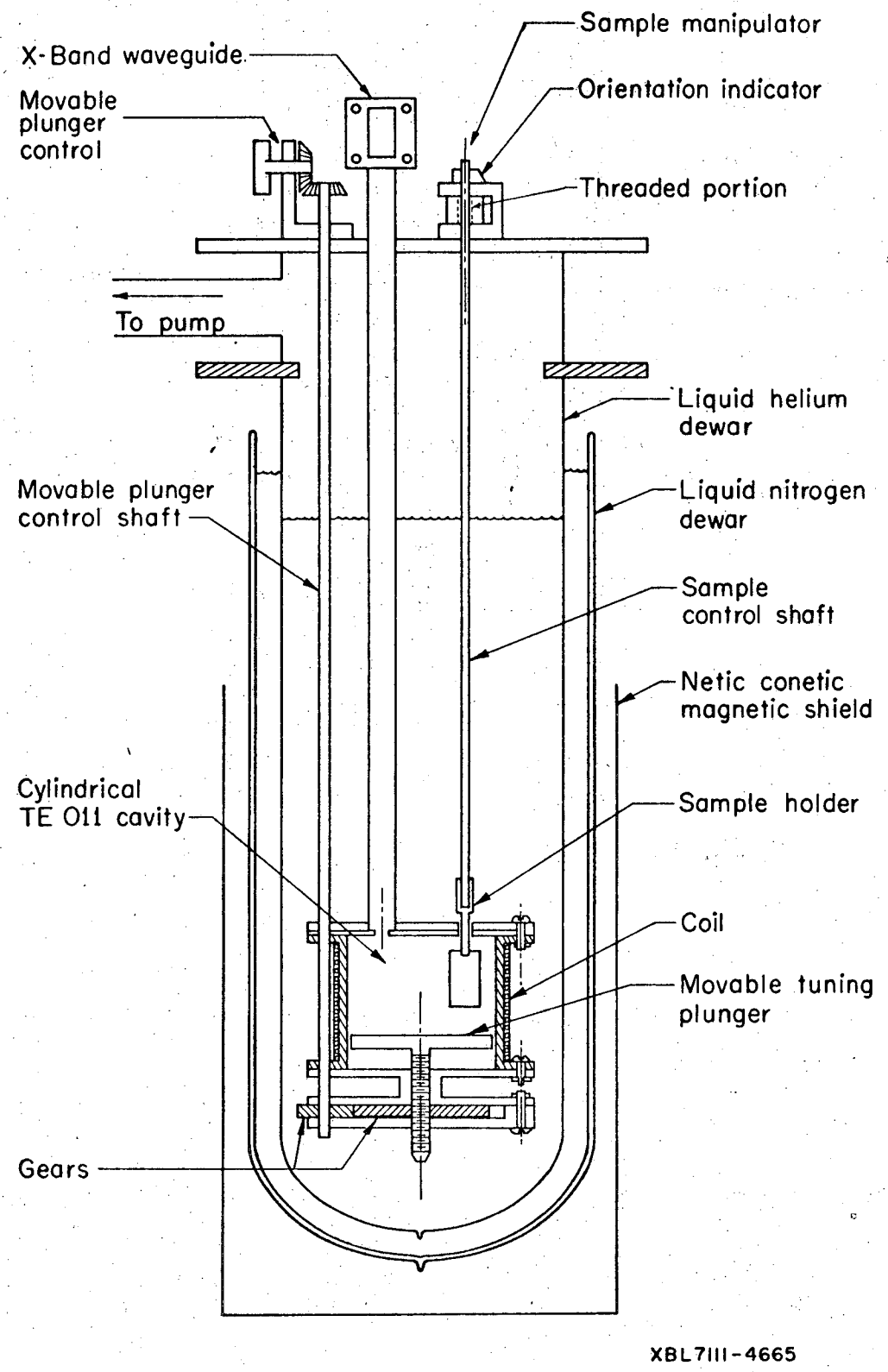
Sample manipulator
X-Band waveguide
Orientation indicator
Movable plunger control
Threaded portion
To pump
Liquid helium dewar
Movable plunger control shaft
Liquid nitrogen dewar
Sample control shaft
Netic conetic magnetic shield
Cylindrical TE 011 cavity
Sample holder
Coil
Movable tuning plunger
Gears
XBL7111-4665

Fig. 1.

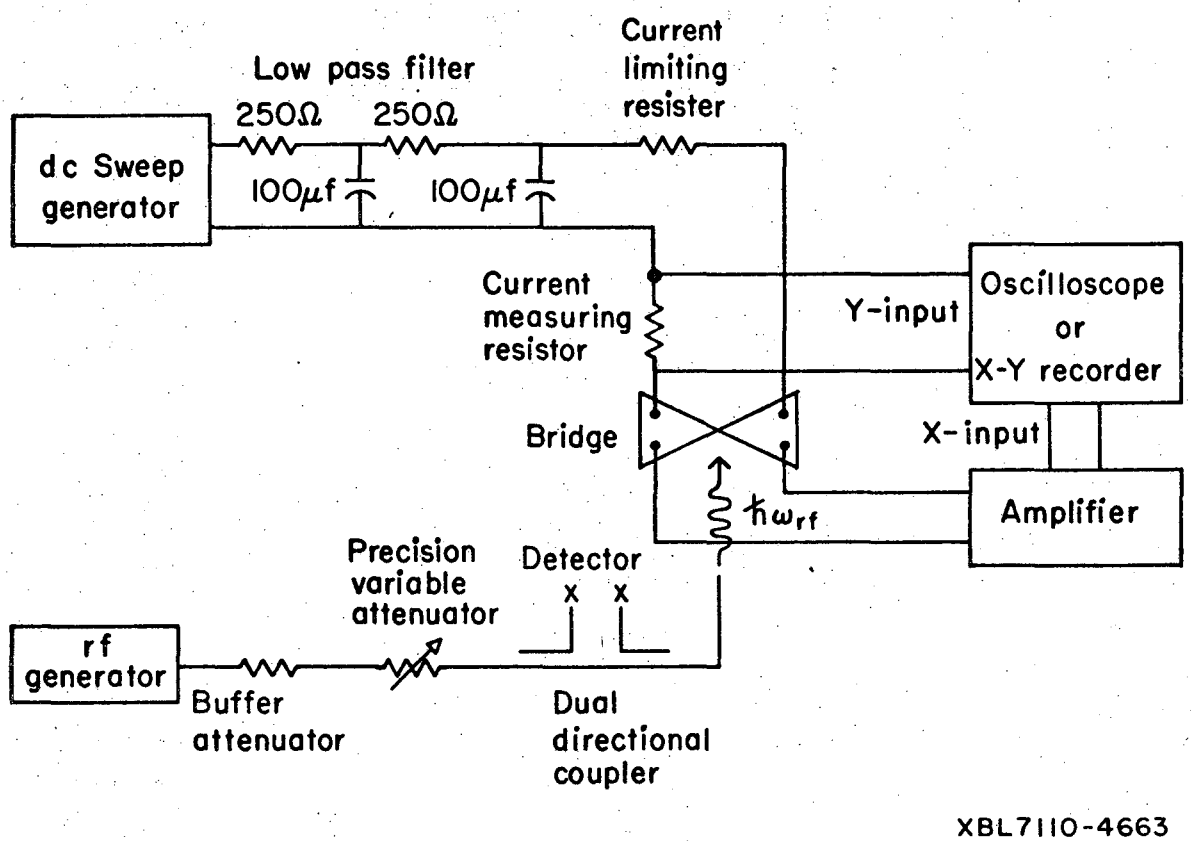
Current
limiting
resister
Low pass filter
250Ω
250Ω
dc Sweep
generator
100μf
100μf
Current
measuring
resistor
Y-input
Oscilloscope
or
X-Y recorder
Bridge
X-input
ħω_rf
Amplifier
Precision
variable
attenuator
Detector
x
x
rf
generator
Buffer
attenuator
Dual
directional
coupler
XBL7110-4663

Fig. 2.

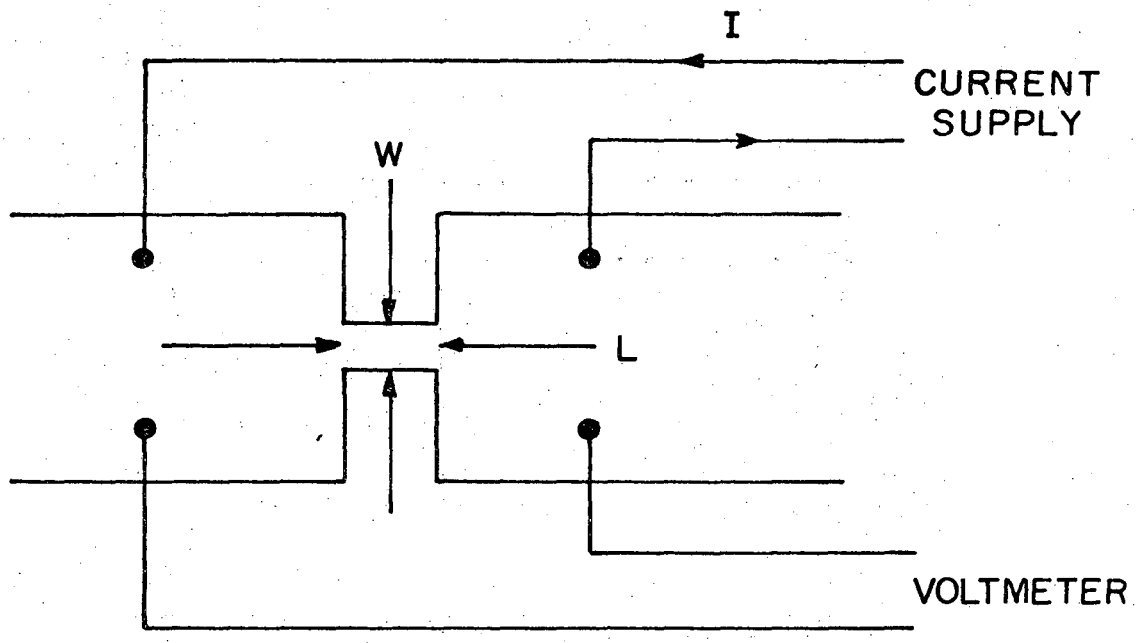

Fig. 3(a)

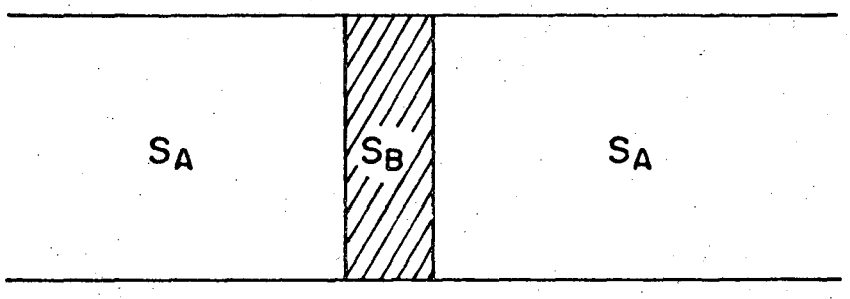

XBL 7111-7530

Fig. 3(b)

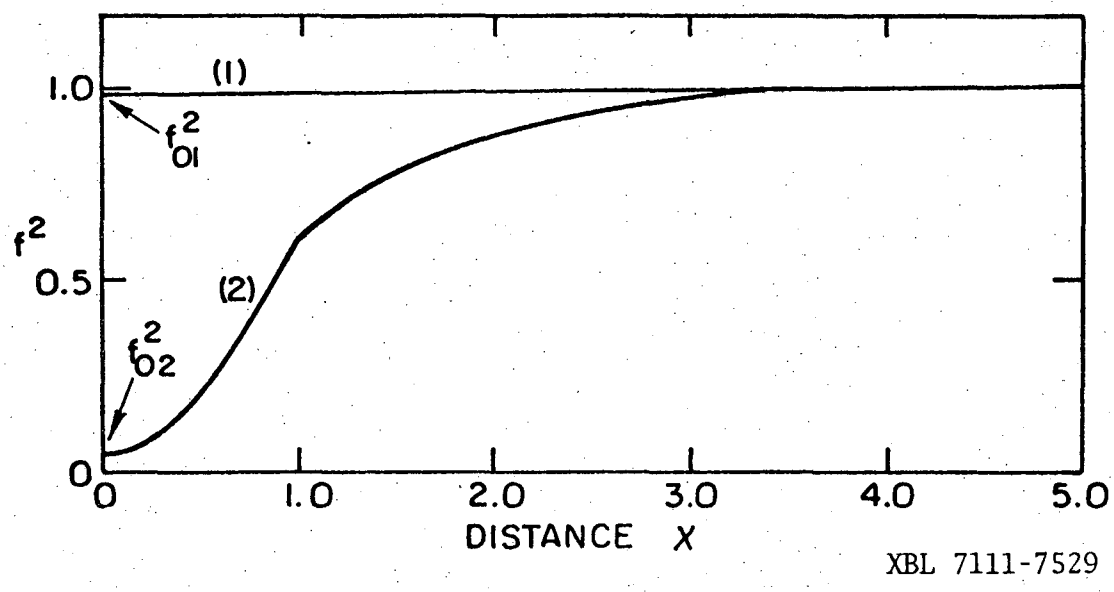

Fig. 4.

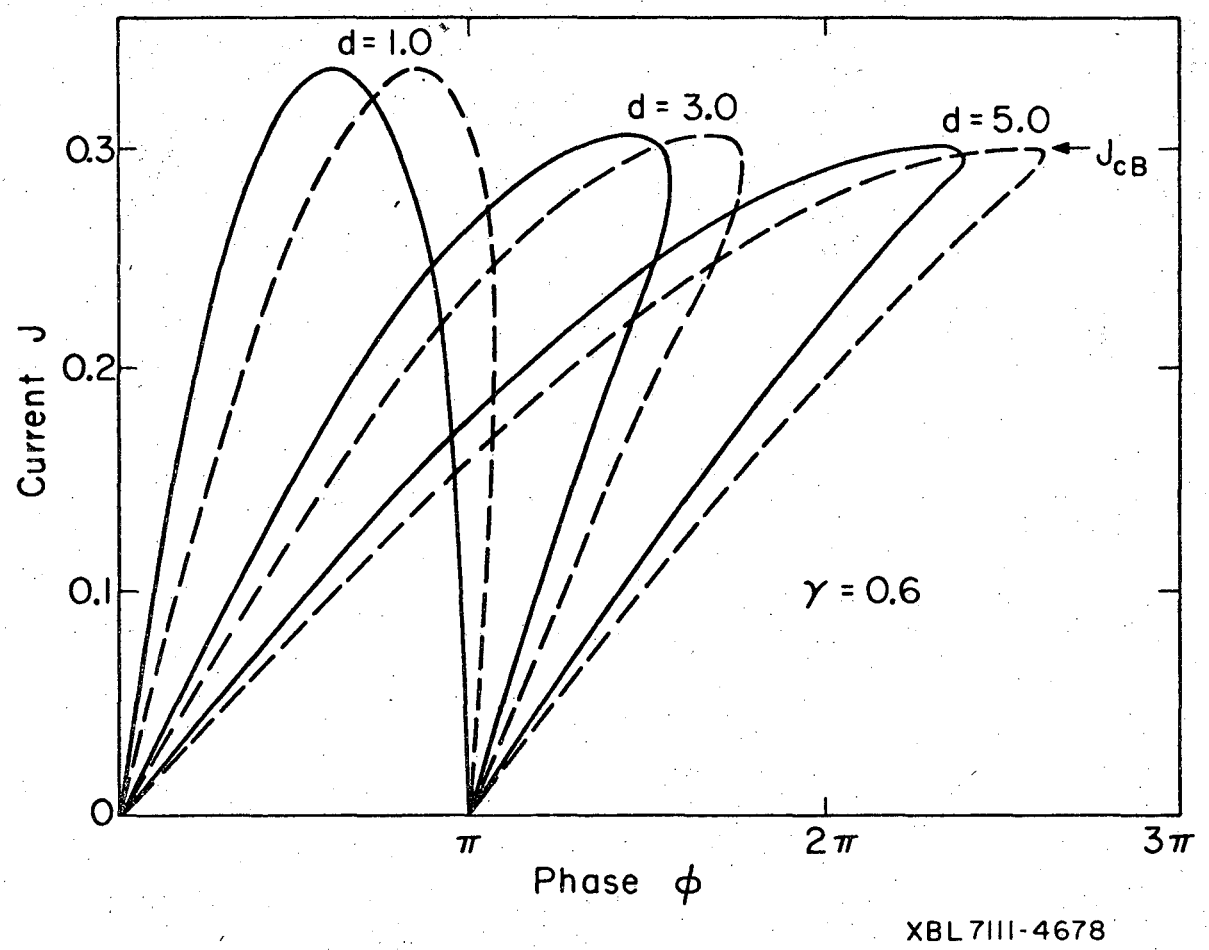
d = 1.0
d = 3.0
d = 5.0
J_{cB}
0.3
0.2
0.1
0
Current J
γ = 0.6
π
2π
3π
Phase ϕ
XBL 7111-4678

Fig. 5.

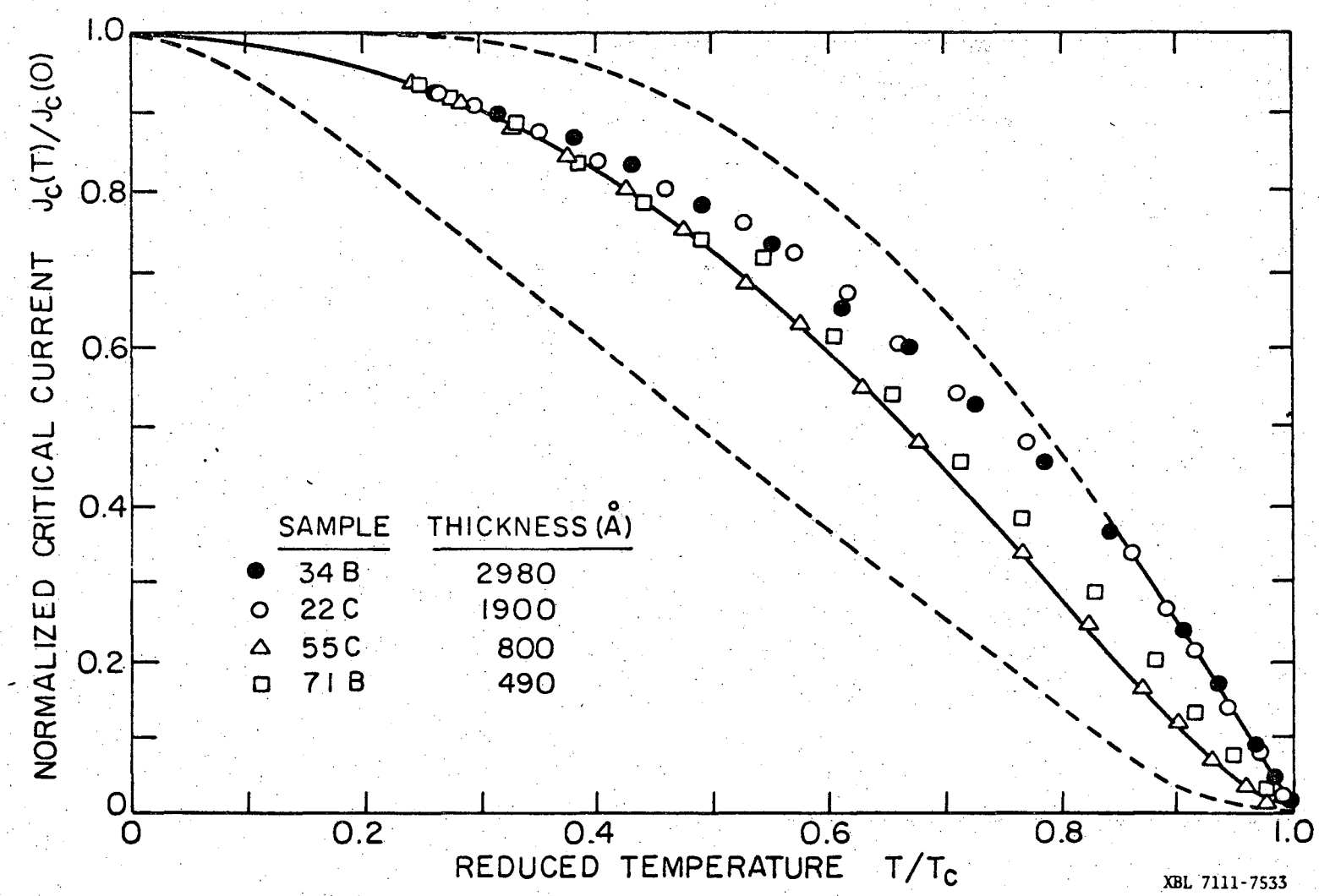
NORMALIZED CRITICAL CURRENT $J_c(T)/J_c(0)$
REDUCED TEMPERATURE T/T_c
0
0.2
0.4
0.6
0.8
1.0
SAMPLE
THICKNESS (Å)
34 B 2980
22 C 1900
55 C 800
71 B 490
XBL 7111-7533

Fig. 6.

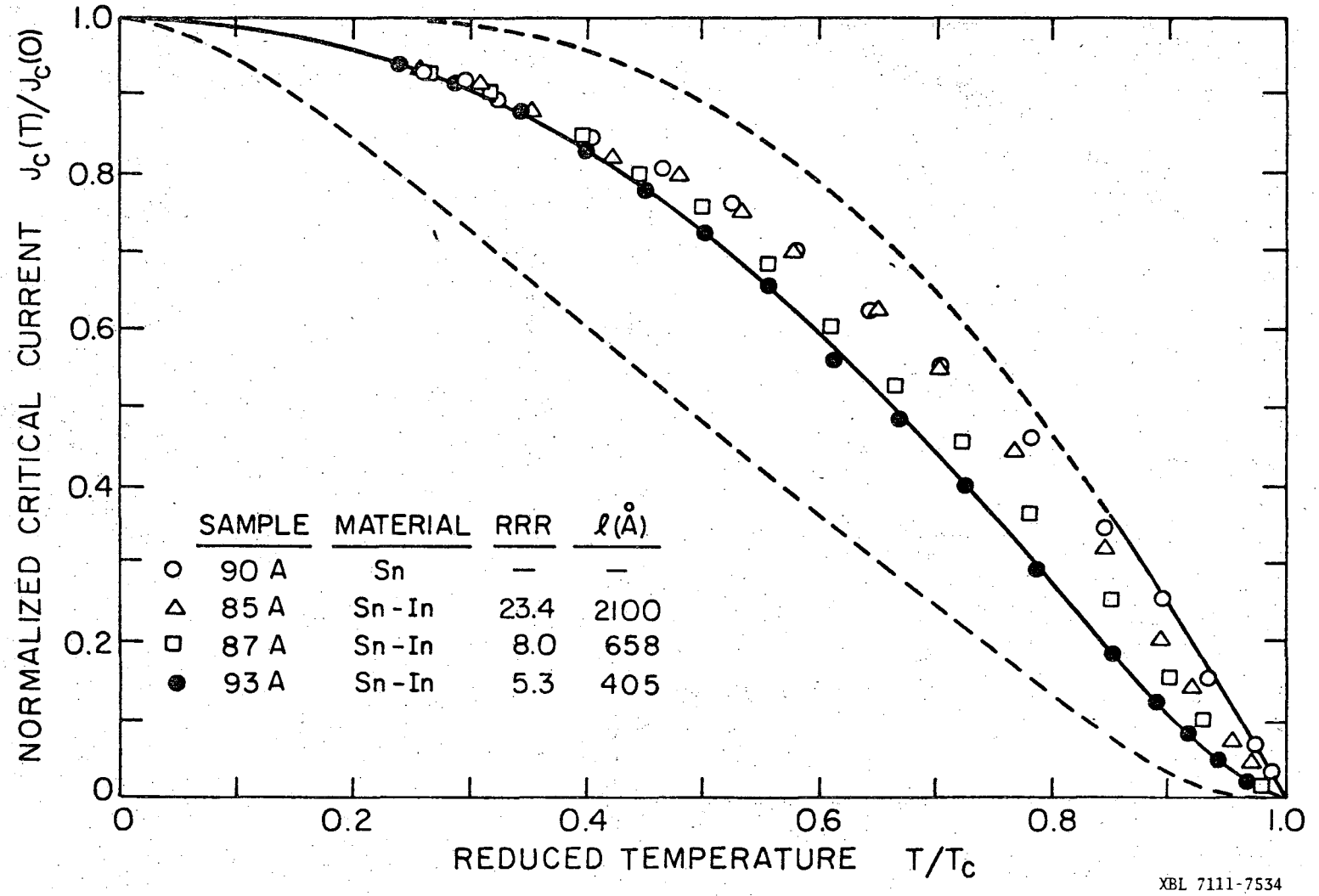
NORMALIZED CRITICAL CURRENT $J_c(T)/J_c(0)$
REDUCED TEMPERATURE T/T_c
0
0.2
0.4
0.6
0.8
1.0
SAMPLE MATERIAL RRR ℓ(Å)
90 A Sn — —
85 A Sn-In 23.4 2100
87 A Sn-In 8.0 658
93 A Sn-In 5.3 405
XBL 7111-7534

Fig. 7.

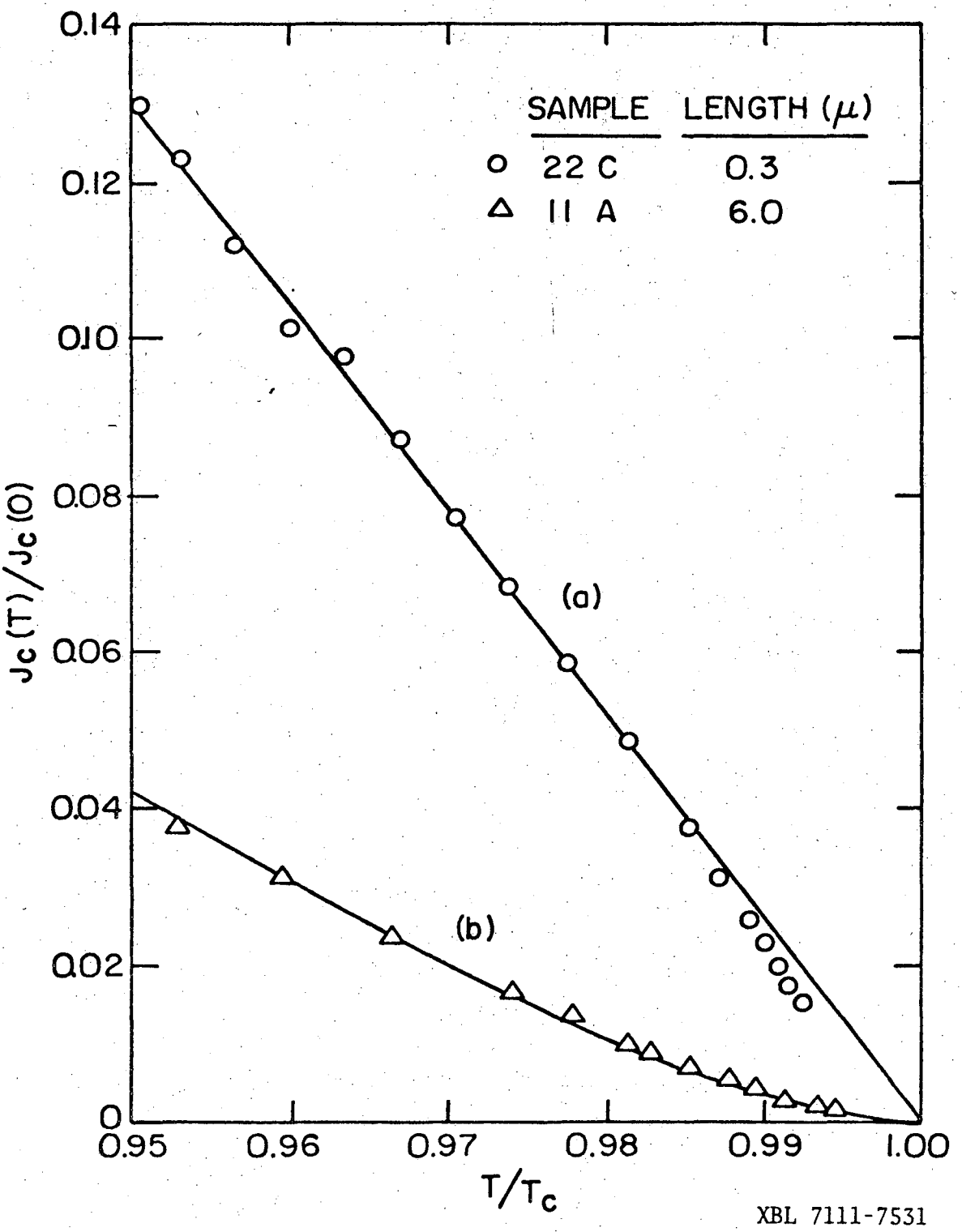
SAMPLE LENGTH (μ)
22 C 0.3
11 A 6.0
(a)
(b)
Jc(T)/Jc(0)
T/Tc
0.14
0.12
0.10
0.08
0.06
0.04
0.02
0
0.95
0.96
0.97
0.98
0.99
1.00
XBL 7111-7531

Fig. 8.

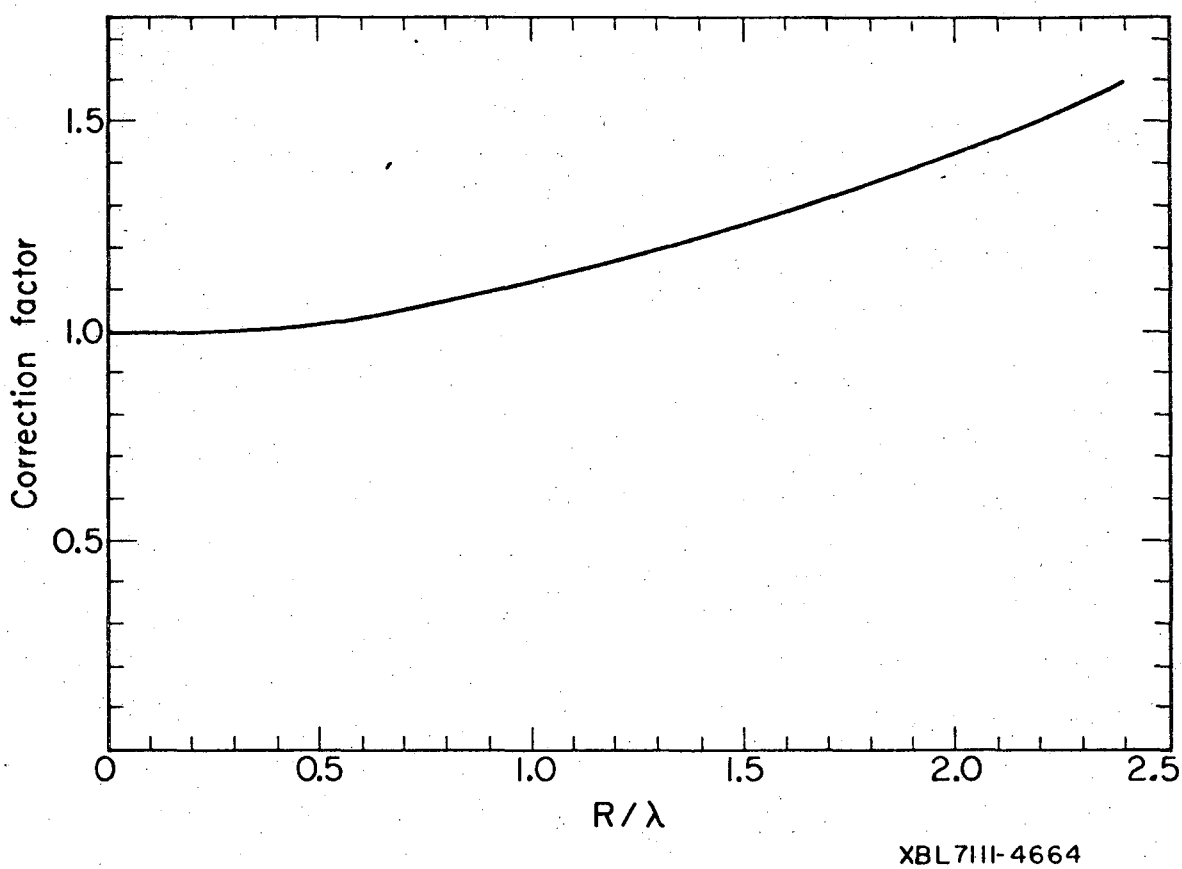

Fig. 9.

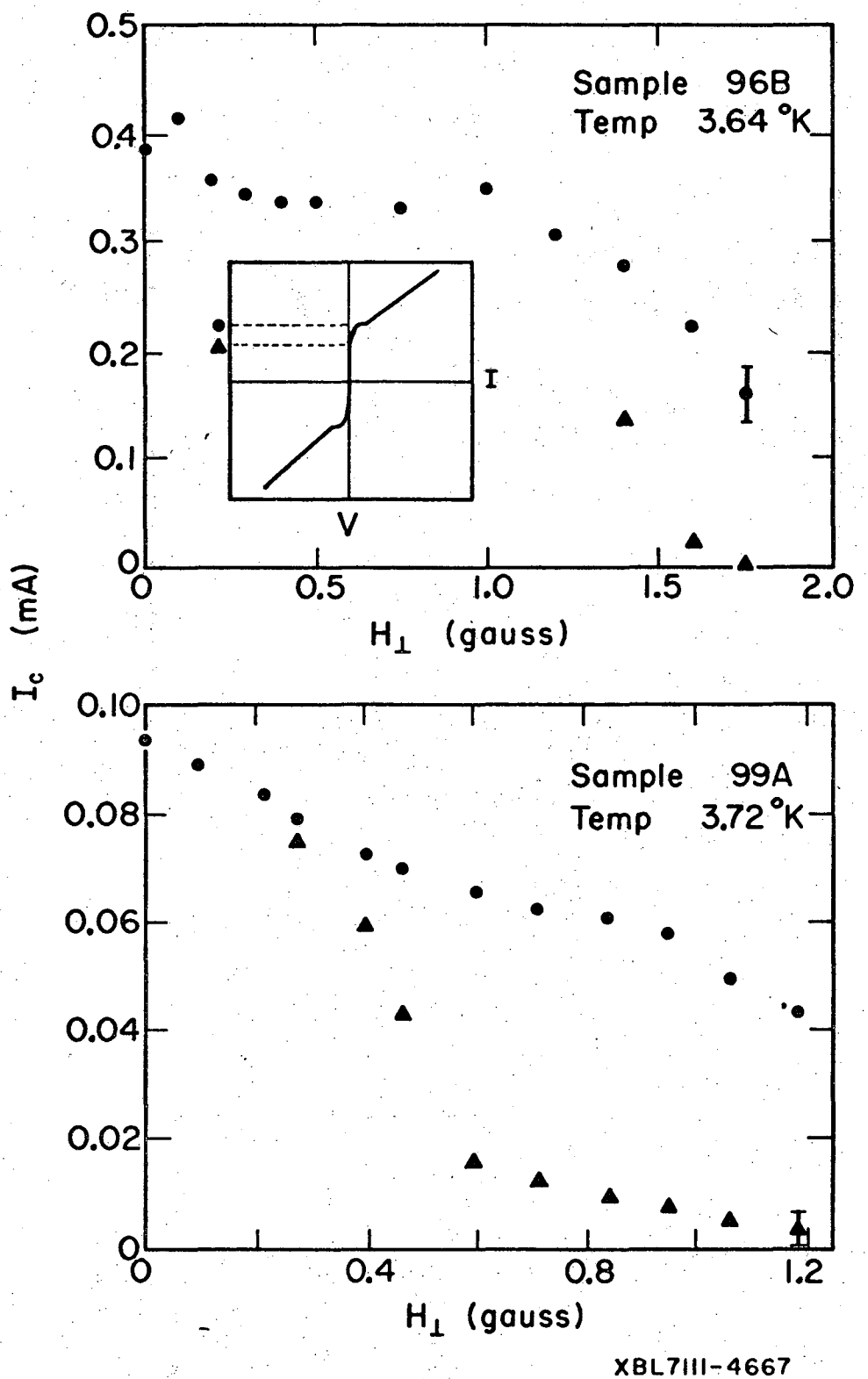
Sample 96B
Temp 3.64 °K
I
V
I_c (mA)
$H_\perp$ (gauss)
Sample 99A
Temp 3.72 °K
$H_\perp$ (gauss)
XBL7111-4667

Fig. 10.

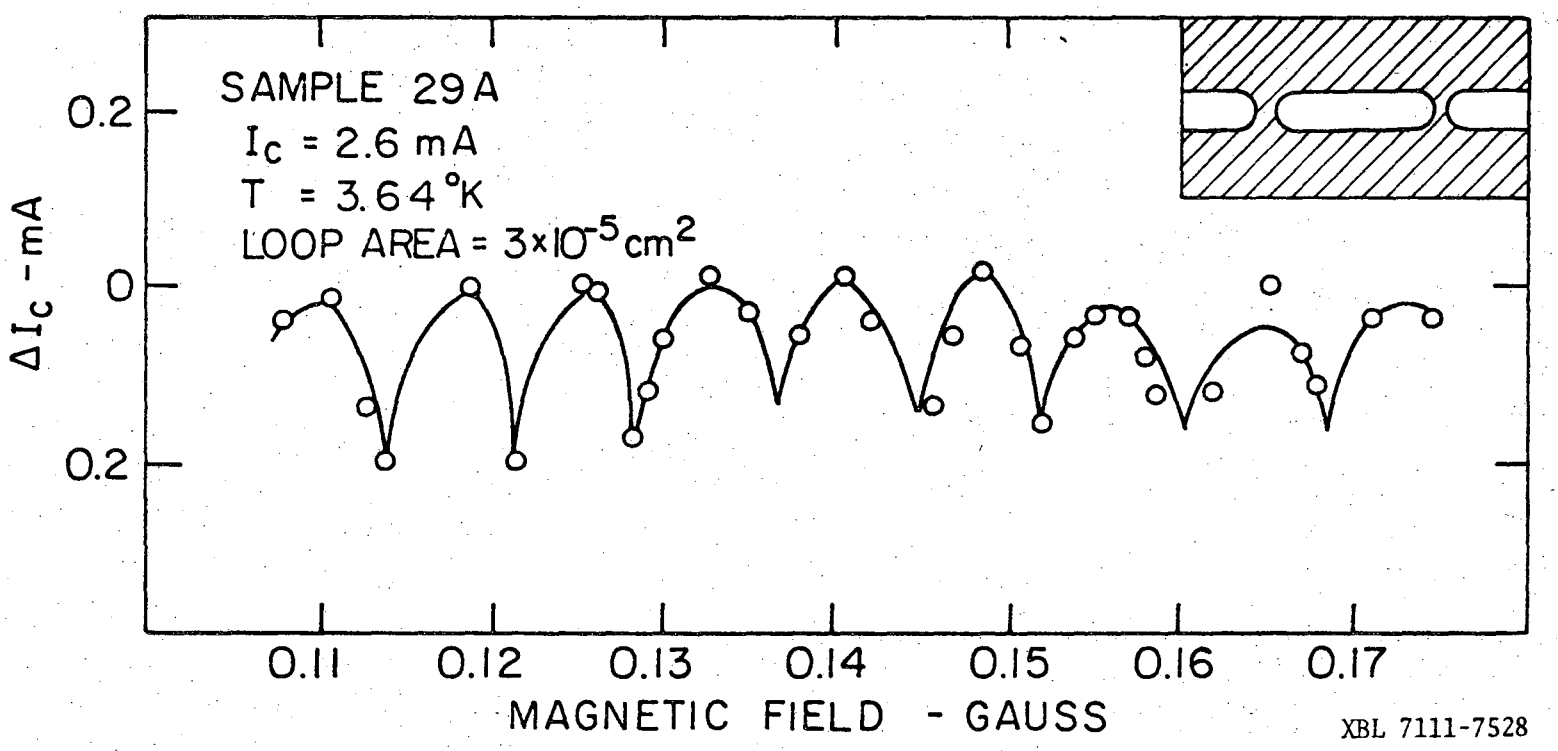
SAMPLE 29A
I_c = 2.6 mA
T = 3.64 °K
LOOP AREA = 3×10^{-5} cm^2
0.2
0
0.2
ΔI_c - mA
0.11
0.12
0.13
0.14
0.15
0.16
0.17
MAGNETIC FIELD - GAUSS
XBL 7111-7528

Fig. 11.

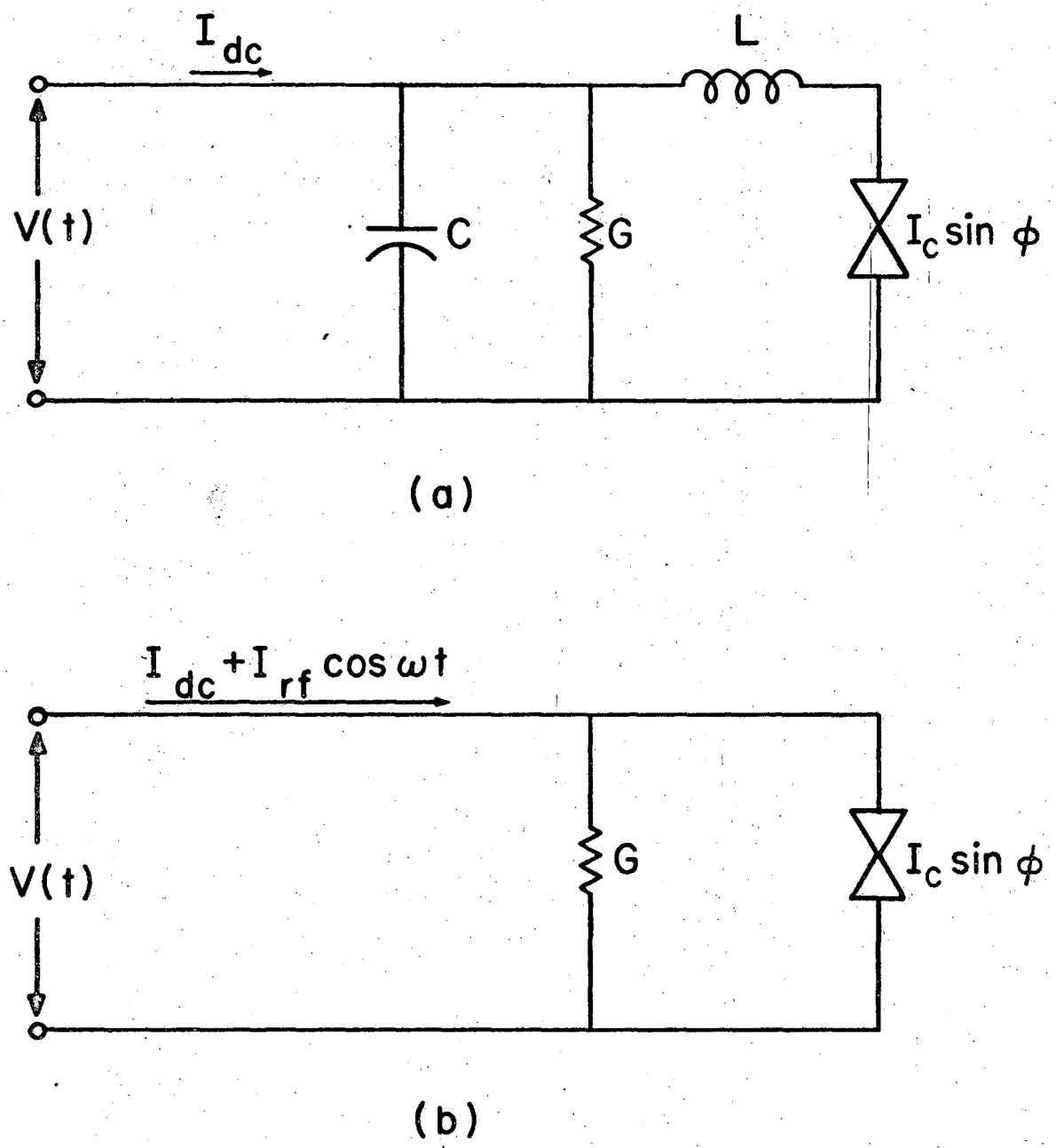

XBL7111-4662

Fig. 12.

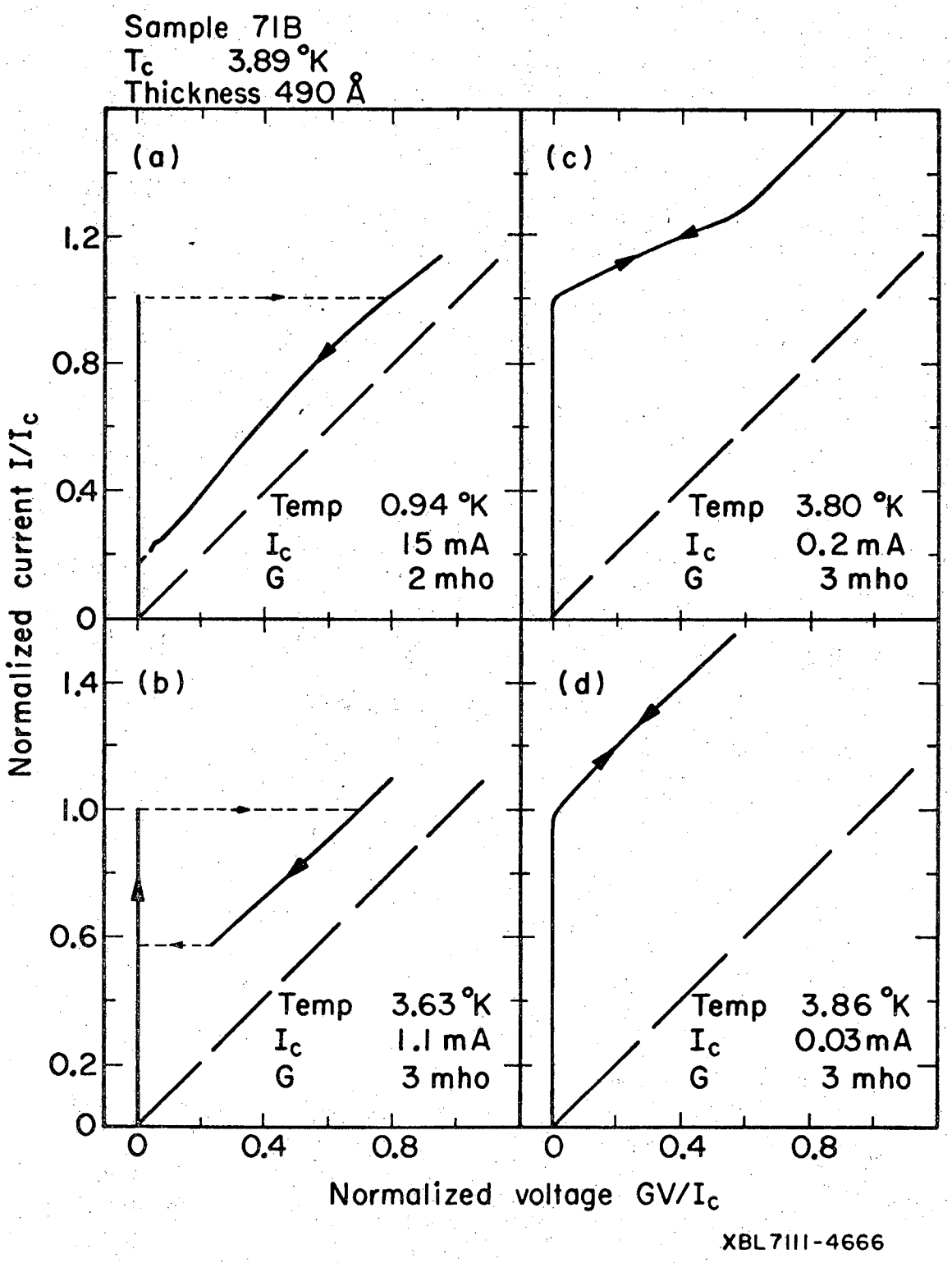
Sample 71B
T_c 3.89 °K
Thickness 490 Å
(a)
Temp 0.94 °K
I_c 15 mA
G 2 mho
(c)
Temp 3.80 °K
I_c 0.2 mA
G 3 mho
(b)
Temp 3.63 °K
I_c 1.1 mA
G 3 mho
(d)
Temp 3.86 °K
I_c 0.03 mA
G 3 mho
Normalized current I/I_c
Normalized voltage GV/I_c
0
0.2
0.4
0.6
0.8
1.0
1.2
1.4
XBL 7111-4666

Fig. 13.

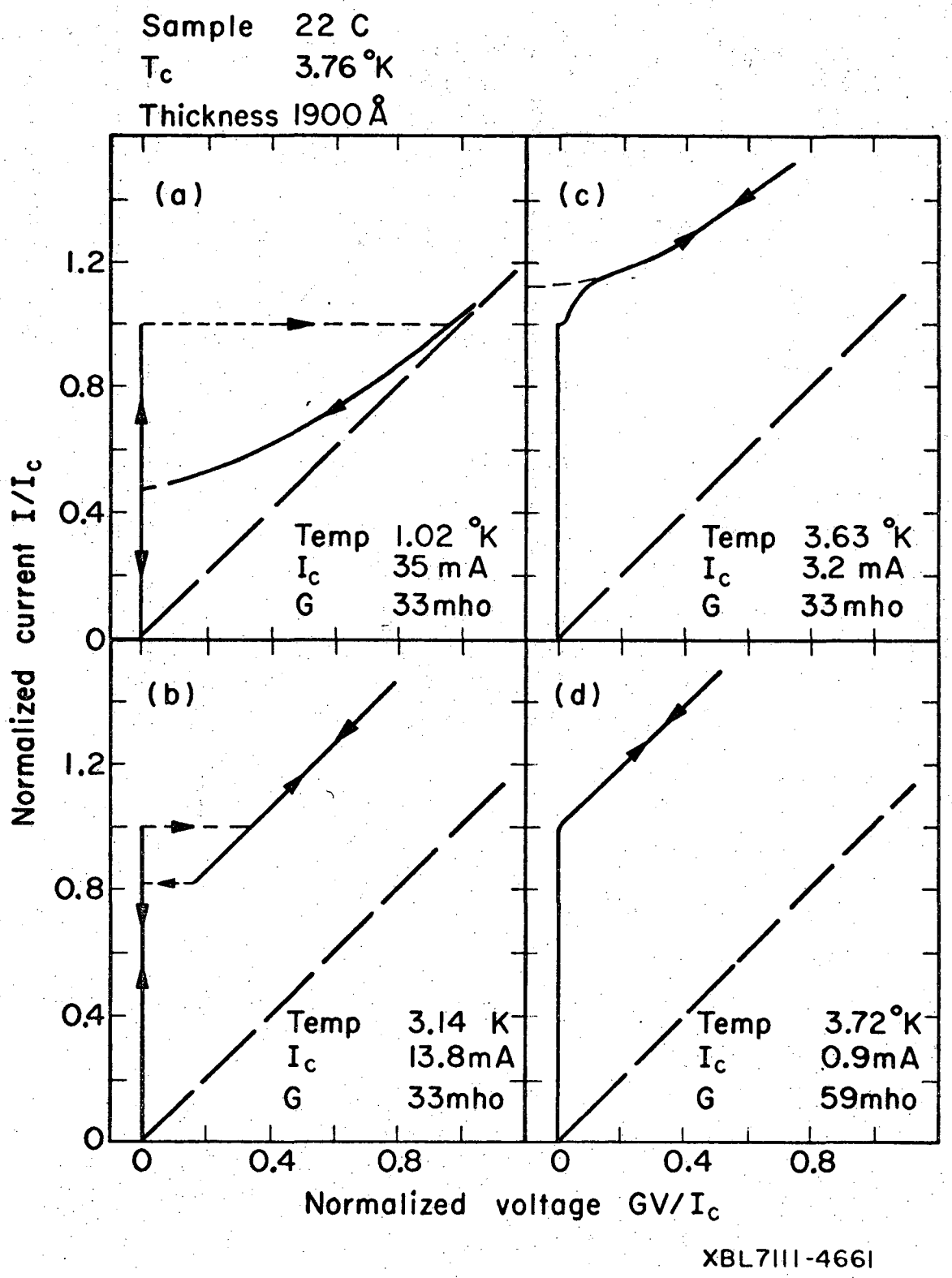
Sample 22 C
T_c 3.76 °K
Thickness 1900 Å
(a)
Temp 1.02 °K
I_c 35 mA
G 33mho
(c)
Temp 3.63 °K
I_c 3.2 mA
G 33mho
(b)
Temp 3.14 K
I_c 13.8mA
G 33mho
(d)
Temp 3.72°K
I_c 0.9mA
G 59mho
Normalized current I/I_c
Normalized voltage GV/I_c
0
0.4
0.8
1.2
XBL7111-4661

Fig. 14.

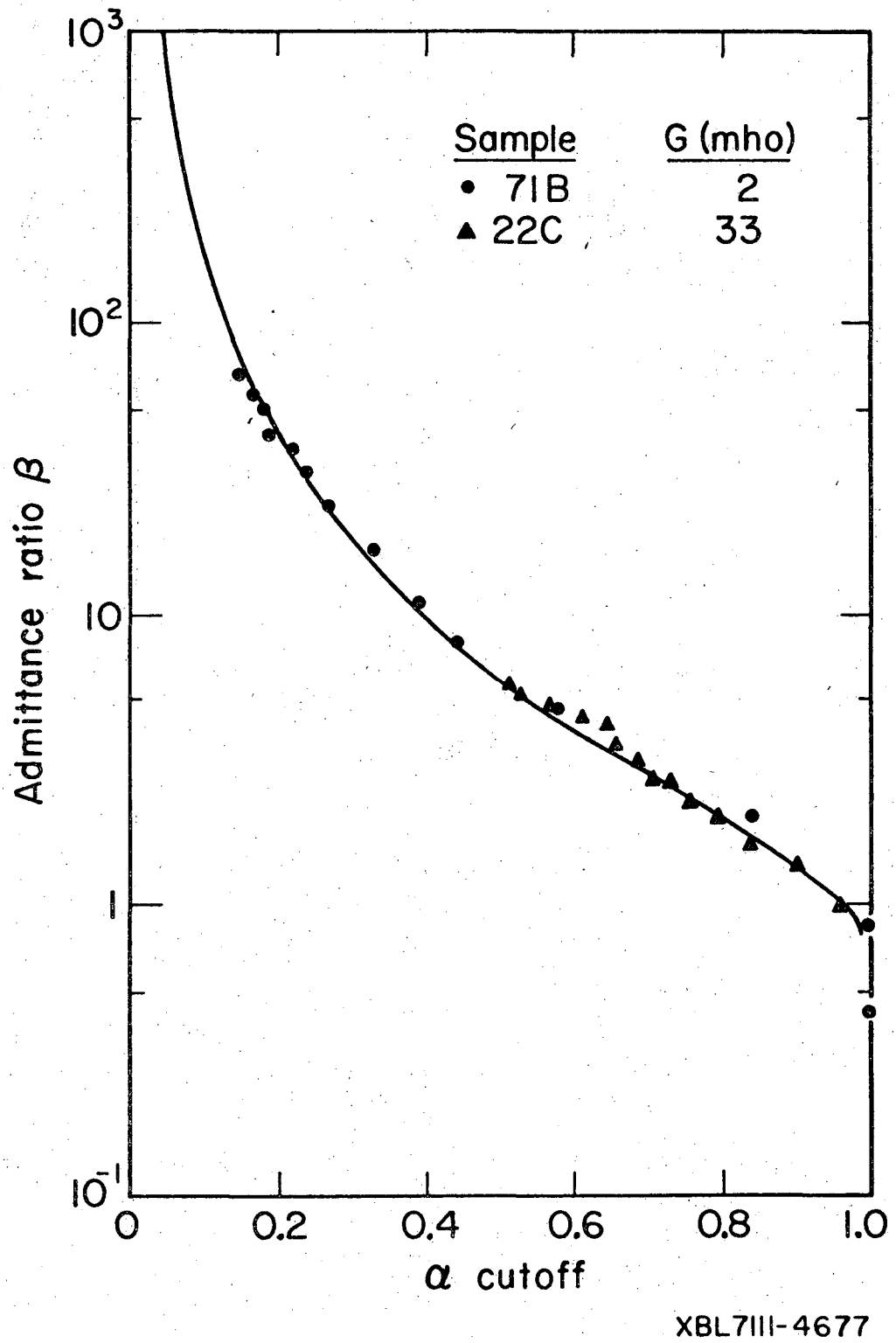
Sample
G (mho)
71B
2
22C
33
Admittance ratio β
α cutoff
10^3
10^2
10
1
10^-1
0
0.2
0.4
0.6
0.8
1.0
XBL7111-4677

Fig. 15.

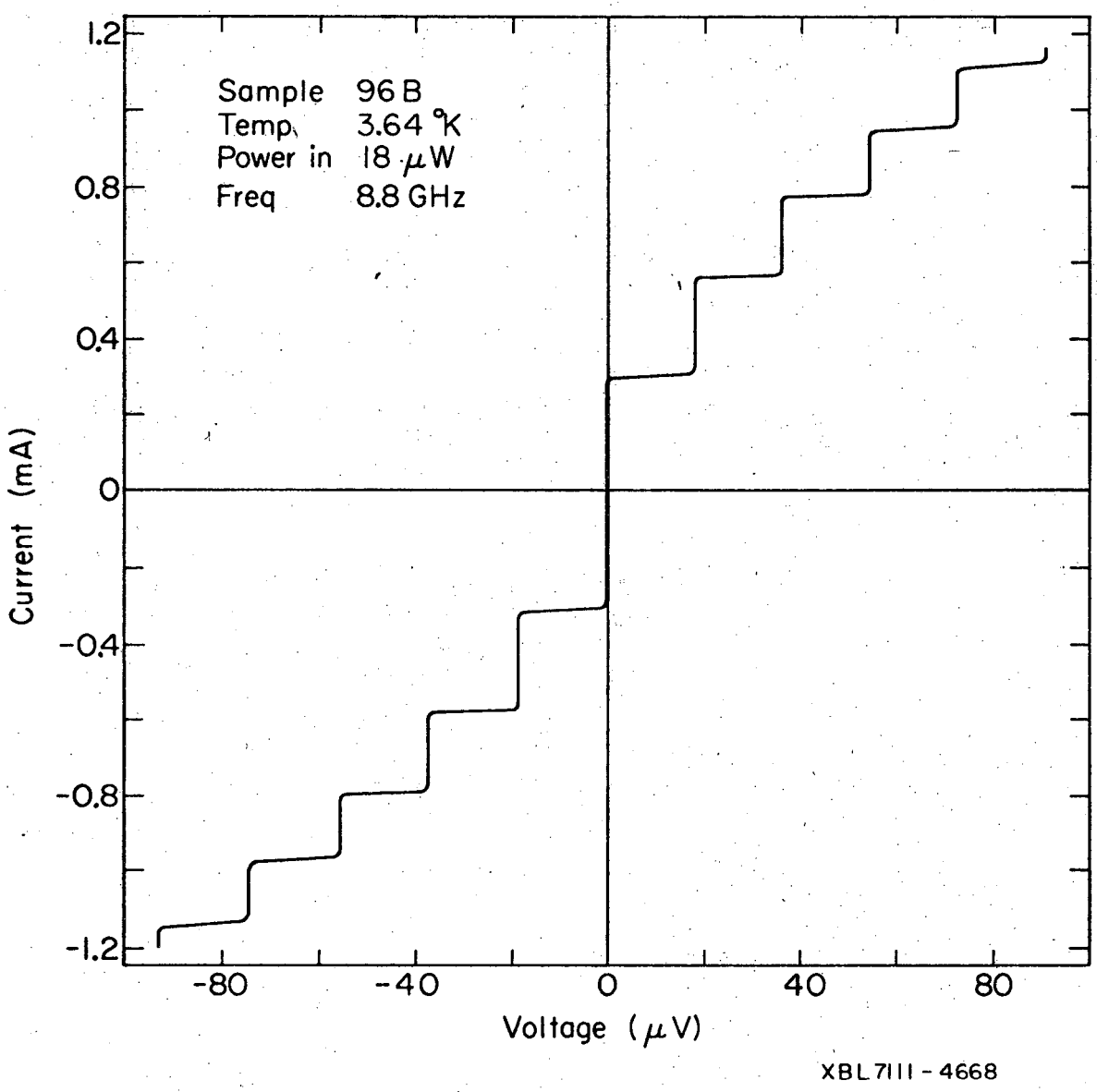
Sample 96 B
Temp. 3.64 °K
Power in 18 μW
Freq 8.8 GHz
1.2
0.8
0.4
0
-0.4
-0.8
-1.2
Current (mA)
-80
-40
0
40
80
Voltage (μV)
XBL 7111 - 4668

Fig. 16.

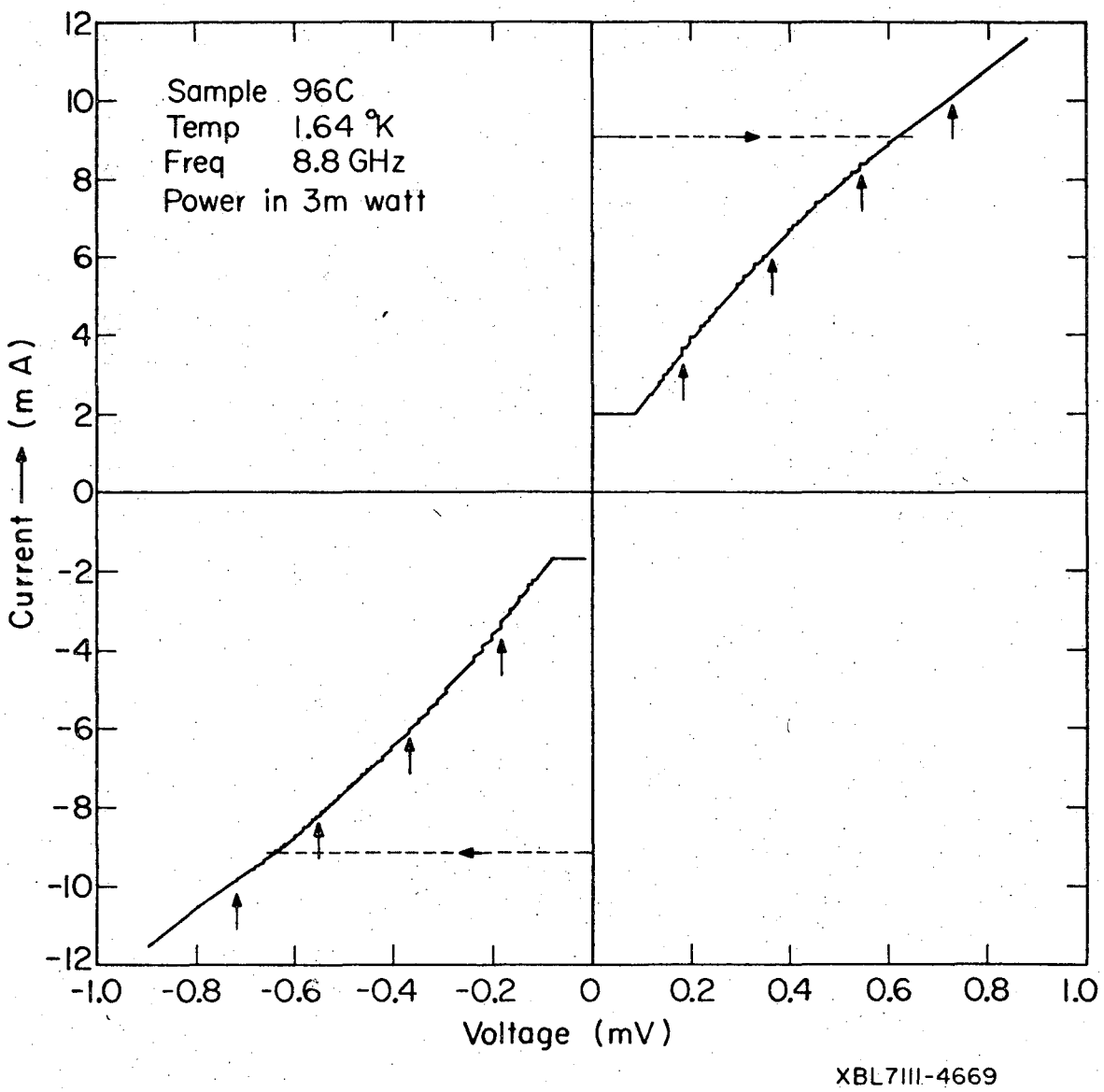
Sample 96C
Temp 1.64 °K
Freq 8.8 GHz
Power in 3m watt
Current ⟶ (m A)
Voltage (mV)
12
10
8
6
4
2
0
-2
-4
-6
-8
-10
-12
-1.0
-0.8
-0.6
-0.4
-0.2
0
0.2
0.4
0.6
0.8
1.0
XBL7111-4669

Fig. 17.

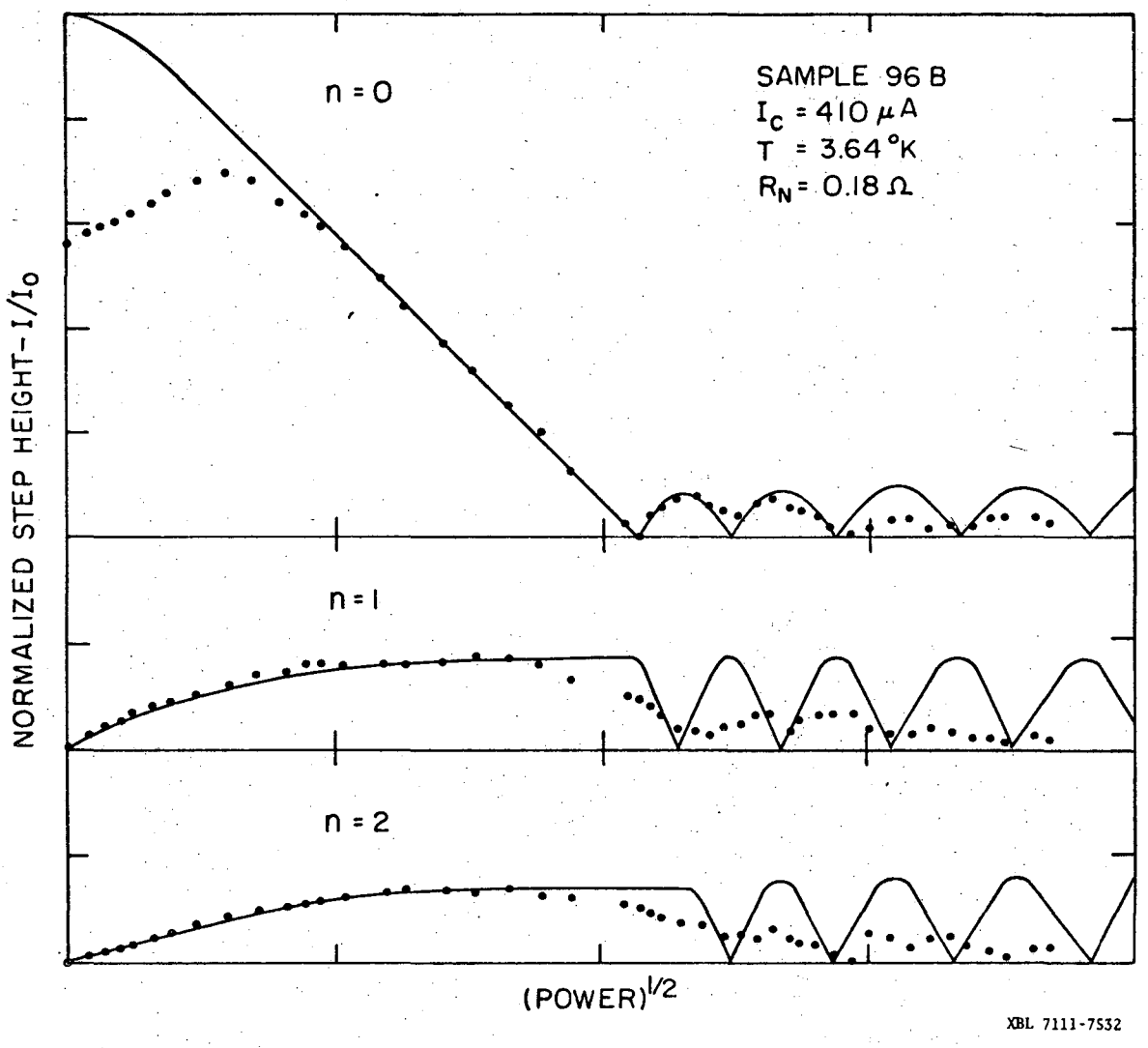
SAMPLE 96 B
I_c = 410 μA
T = 3.64 °K
R_N = 0.18 Ω
n = 0
n = 1
n = 2
NORMALIZED STEP HEIGHT- I/I_0
$(POWER)^{1/2}$
XBL 7111-7532

Fig. 18.

LEGAL NOTICE

This report was prepared as an account of work sponsored by the United States Government. Neither the United States nor the United States Atomic Energy Commission, nor any of their employees, nor any of their contractors, subcontractors, or their employees, makes any warranty, express or implied, or assumes any legal liability or responsibility for the accuracy, completeness or usefulness of any information, apparatus, product or process disclosed, or represents that its use would not infringe privately owned rights.

TECHNICAL INFORMATION DIVISION
LAWRENCE BERKELEY LABORATORY
UNIVERSITY OF CALIFORNIA
BERKELEY, CALIFORNIA 94720